Dynamin photoinactivation blocks Clathrin and α-adaptin recruitment and induces bulk membrane retrieval

Jaroslaw Kasprowicz,[1,2,3] Sabine Kuenen,[1,2,3] Jef Swerts,[1,2,3] Katarzyna Miskiewicz,[1,2,3] and Patrik Verstreken[1,2,3]

[1]VIB Center for the Biology of Disease, [2]Laboratory of Neuronal Communication, Department for Human Genetics, and [3]Leuven Institute for Neurodegenerative Diseases, KU Leuven, 3000 Leuven, Belgium

Dynamin is a well-known regulator of synaptic endocytosis. Temperature-sensitive *dynamin* (*shi*^{ts1}) mutations in *Drosophila melanogaster* or deletion of some of the mammalian Dynamins causes the accumulation of invaginated endocytic pits at synapses, sometimes also on bulk endosomes, indicating impaired membrane scission. However, complete loss of *dynamin* function has not been studied in neurons in vivo, and whether Dynamin acts in different aspects of synaptic vesicle formation remains enigmatic. We used acute photoinactivation and found that loss of Dynamin function blocked membrane recycling and caused the buildup of huge membrane-connected cisternae, in contrast to the invaginated pits that accumulate in *shi*^{ts1} mutants. Moreover, photoinactivation of Dynamin in *shi*^{ts1} animals converted these pits into bulk cisternae. Bulk membrane retrieval has also been seen upon Clathrin photoinactivation, and superresolution imaging indicated that acute Dynamin photoinactivation blocked Clathrin and α-adaptin relocalization to synaptic membranes upon nerve stimulation. Hence, our data indicate that Dynamin is critically involved in the stabilization of Clathrin- and AP2-dependent endocytic pits.

Introduction

During intense neuronal activity, synapses need to recycle synaptic vesicles to maintain neuronal communication. The best studied route for vesicle regeneration in neurons is Clathrin-mediated endocytosis (CME) but also bulk membrane uptake participates to recycle membrane (Holt et al., 2003; LoGiudice and Matthews, 2006; Watanabe et al., 2013; Winther et al., 2013). During CME, lipids, adaptors, and accessory proteins initiate vesicle formation (McMahon and Boucrot, 2011). In parallel, Clathrin, polymerized into cages, serves as a "mold" for new synaptic vesicles, preventing excessive membrane uptake and ensuring uniform vesicle size (Heerssen et al., 2008; Kasprowicz et al., 2008). Although numerous proteins have been implicated in CME, the exact molecular mechanisms by which these components coordinate the formation of new vesicles remains incompletely understood.

Dynamin is a large GTPase that is implicated in vesicle endocytosis in neuronal and nonneuronal cells (van der Bliek and Meyerowitz, 1991; Liu et al., 1998, 2011; Damke et al., 2001; Marks et al., 2001; Chen et al., 2002; Narayanan et al., 2005; Macia et al., 2006; Aguet et al., 2013). The protein binds to accessory endocytic proteins and lipids (David et al., 1996; Okamoto et al., 1997; Qualmann et al., 1999; Simpson et al., 1999; Bethoney et al., 2009; Sundborger et al., 2011), and in GTP-bound state, it assembles into rings at the base of deeply invaginated pits (Chen et al., 2002; Macia et al., 2006; Liu et al., 2011). GTP hydrolysis then induces conformational changes (Roux et al., 2006; Bashkirov et al., 2008; Chappie et al., 2010; Ford et al., 2011) that result in the separation of the vesicle and plasma membrane (McNiven et al., 2000); at the synapse, this process generates new vesicles that can participate in a new round of neurotransmitter release (Ferguson and De Camilli, 2012). Consistent with a role in membrane scission in vitro, temperature-sensitive *dynamin* fly mutants

J. Kasprowicz and S. Kuenen contributed equally to this paper.

Correspondence to Patrik Verstreken: patrik.verstreken@med.kuleuven.be

Abbreviations used in this paper: α-Ada, α-adaptin; ANOVA, analysis of variance; a.u., arbitrary unit; Chc, Clathrin heavy chain; Clc, Clathrin light chain; CME, Clathrin-mediated endocytosis; DLG, disc large; EJC, excitatory junctional current; EJP, excitatory junctional potential; FALI, fluorescein-assisted light inactivation; NMJ, neuromuscular junction; TEM, transmission EM.

The Rockefeller University Press $30.00
J. Cell Biol. Vol. 204 No. 7 1141–1156
www.jcb.org/cgi/doi/10.1083/jcb.201310090

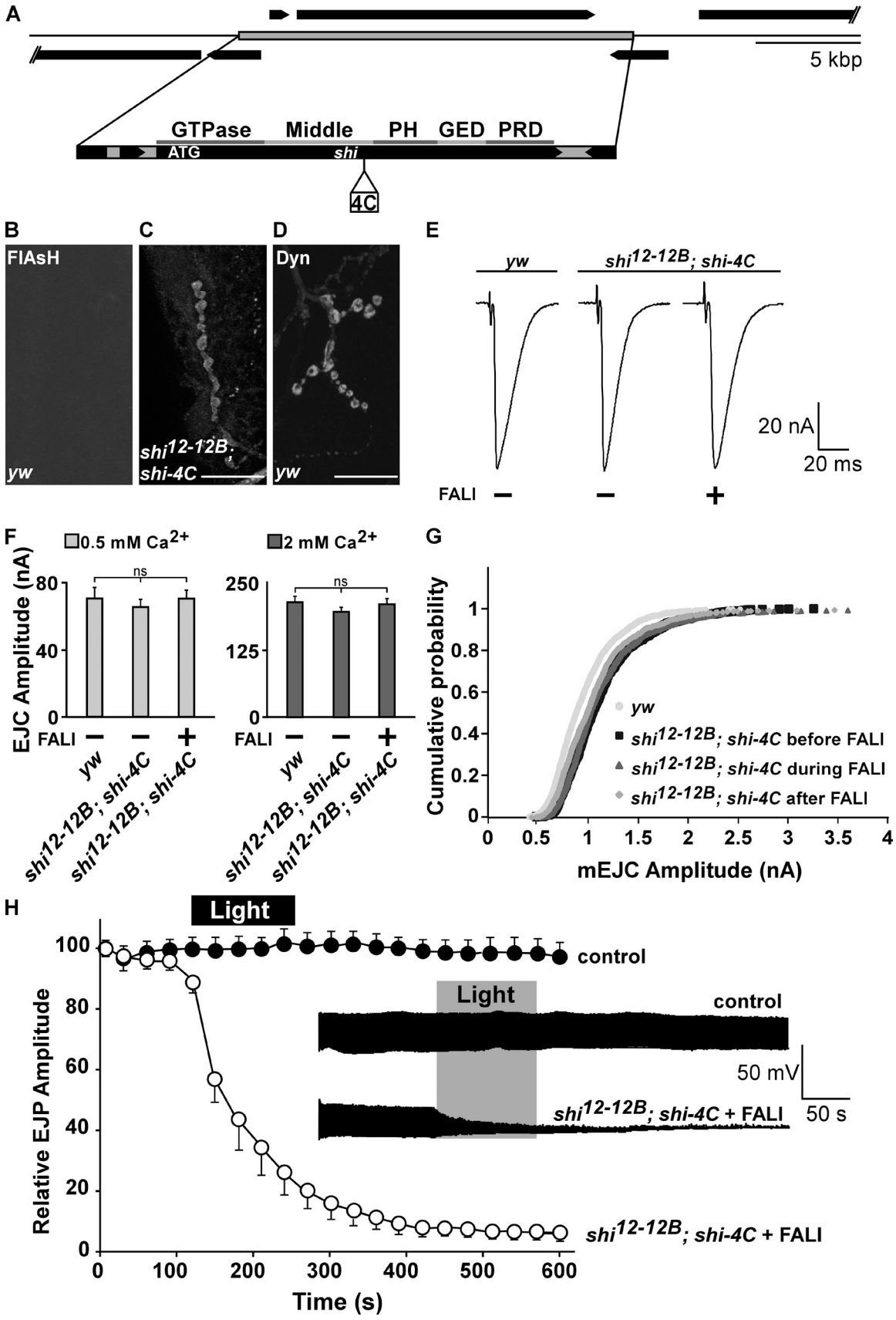

Figure 1. **Photoinactivation of Dynamin blocks synaptic vesicle recycling.** (A) Genomic *dynamin* construct tagged in the middle domain with a Flag-tetracysteine tag (*shi-4C*). PH, Pleckstrin homology; PRD, Proline-rich domain; GED, GTPase effector domain. (B–D) FlAsH fluorescence after incubation of *yw* controls (B) and *shi*$^{12\text{-}12B}$*; shi-4C* (C) third instar fillets in FlAsH reagent shows labeling only in boutons of animals expressing Shi-4C (C). (D) Anti-Dynamin

(shi^{ts1}) that were stimulated at restrictive temperature show a depletion of synaptic vesicles and numerous deeply invaginated pits that are stuck at the plasma membrane (Koenig and Ikeda, 1989; Chen et al., 1991, 2002; van der Bliek and Meyerowitz, 1991). Likewise, in mammalian neurons in which either one or two of the three Dynamin isoforms were deleted, a massive accumulation of invaginated pits is observed (Ferguson et al., 2007; Hayashi et al., 2008; Raimondi et al., 2011; Park et al., 2013). These studies in neurons indicate that a critical role for Dynamin in synaptic vesicle formation is to facilitate membrane fission. However, these genetic conditions in mice and flies may still retain some aspects of Dynamin function, and it is currently unclear whether low levels of the second or third Dynamin isoform in mice or the presence of the temperature-sensitive Dynamin protein (Shi^{ts1}) in flies at a restrictive temperature is concealing potential additional functions for the protein in synaptic vesicle formation.

In this work, we use acute and specific fluorescein-assisted light inactivation (FALI) of Dynamin to study endocytosis in the absence of Dynamin function. Surprisingly, loss of Dynamin function does not cause the accumulation of deeply invaginated pits, as seen in shi^{ts1} mutants; instead, it results in the accumulation of giant bulk cisternae that can fill entire synaptic boutons and do not significantly participate in the synaptic vesicle cycle. Similarly, photoinactivation of Dynamin in shi^{ts1} mutants at restrictive temperature does not result in the accumulation of invaginated pits but in the formation of massive membrane-attached bulk cisternae, indicating that shi^{ts1} retains the ability to prevent bulk endocytosis. Furthermore, these defects in membrane uptake are very reminiscent of those seen in *clathrin* mutant synapses with photoinactivated Clathrin, and we therefore used superresolution imaging to localize Clathrin heavy chain (Chc) and the Clathrin adaptor subunit α-adaptin (α-Ada) at stimulated synaptic boutons. In contrast to controls, at neuromuscular junctions (NMJs) in which Dynamin was photoinactivated, Chc and α-Ada both fail to relocalize to and concentrate in the bouton periphery close to the presynaptic plasma membrane. Our data indicate that Dynamin is critical to coordinate Clathrin- and α-Ada–dependent steps during synaptic vesicle budding, and this function is retained in temperature-sensitive shi^{ts1} mutants.

Results

Synapses with photoinactivated Dynamin do not maintain neurotransmitter release during intense stimulation

Whereas mammals harbor three *dynamin* genes, *Drosophila melanogaster* harbors only one, *shi* (*shibire*; Cao et al., 1998). *shi*-null mutants ($shi^{12\text{-}12B}$) die as embryos (Grant et al., 1998), precluding us from analyzing defects in synaptic function. To circumvent issues with early lethality or development, we resorted to acute FlAsH (4′,5′-bis[1,3,2-dithioarsolan-2-yl] fluorescein)-mediated FALI (FlAsH-FALI; Marek and Davis, 2002), a technology already used to inactivate Synaptotagmin I (Poskanzer et al., 2003), Chc (Kasprowicz et al., 2008), and Clathrin light chain (Clc; Heerssen et al., 2008) at the *Drosophila* NMJ. Using recombineering in *Escherichia coli*, we retrieved the *shi* gene from BACR32K23 into P[acman] (Venken et al., 2006), and we then recombineered a 16–amino acid tetracysteine (4C) tag into the middle domain of Dynamin (Shi-4C; Fig. 1 A; Venken et al., 2008). We tagged the middle domain of Dynamin because FALI at this site would ensure Dynamin as well as Dynamin complex photoinactivation. The middle domain is part of a stalk in the quaternary structure of Dynamin. This stalk is required to form dimers that are used as building units in the formation of Dynamin rings that assemble around the necks of newly forming vesicles (Chappie et al., 2010; Gao et al., 2010; Ford et al., 2011). We find that the *shi-4C* construct expressed under endogenous promoter control in $shi^{12\text{-}12B}$–null mutants ($shi^{12\text{-}12B}$; *shi-4C*) localizes at boutons very similarly to endogenous Dynamin (Fig. 1, B–D).

Assessing whether Shi-4C is functional, we find that the presence of Shi-4C fully rescues the lethality associated with $shi^{12\text{-}12B}$–null mutants, and these rescued animals do not show obvious behavioral or developmental defects (Fig. S1, A and B). Moreover, $shi^{12\text{-}12B}$; *shi-4C* animals show normal synaptic NMJ morphology (Fig. S1, C–E). In addition, excitatory junctional currents (EJCs) and excitatory junctional potentials (EJPs) recorded from $shi^{12\text{-}12B}$; *shi-4C* animals in different external calcium concentrations (Fig. 1, E–H) elicited at low (1 Hz; Fig. 1, E and F) or high (10 Hz; Fig. 1 H, first 2 min) frequency nerve stimulation are comparable to controls. Finally, also, the amplitude distribution of spontaneous vesicle fusion events in $shi^{12\text{-}12B}$; *shi-4C* is very similar to controls (Fig. 1 G). Hence, Shi-4C constitutes a functional protein that recapitulates normal Dynamin function.

Next, we tested whether photoinactivation of the 4C-tagged Dynamin affects neurotransmitter release during low and high frequency stimulation. Shi-4C in $shi^{12\text{-}12B}$; *shi-4C* animals was loaded with FlAsH, and EJCs were measured before and after 2 min of 508-nm light inactivation. As shown in Fig. 1 (E–G), the amplitude of EJCs recorded at low frequency stimulation in 0.5 or 2 mM calcium and miniature EJC amplitude recorded in 0.5 mM calcium before (Fig. 1, E and F, −FALI) and after (Fig. 1, E and F, +FALI) Dynamin photoinactivation are very similar. In contrast, during more intense (10 Hz) stimulation, Dynamin photoinactivation (2 min of 508-nm light) results in a fast drop of the EJP amplitude and most recordings reach 0 in <5 min after photoinactivation (Fig. 1 H), very similar to recordings made from

(Dyn) labeling in *yw* animals. Bars, 20 µm. (E) Sample EJC traces recorded from muscle 6 in 0.5 mM of extracellular $CaCl_2$ in *yw* controls and $shi^{12\text{-}12B}$; *shi-4C* animals that were not subjected to FALI (−) and $shi^{12\text{-}12B}$; *shi-4C* after FALI (+). (F) Quantification of the EJC amplitude recorded in 0.5 and 2 mM $CaCl_2$ in controls *yw* and $shi^{12\text{-}12B}$; *shi-4C* without (−) and with FALI (+). Error bars show SEMs; ANOVA (post hoc Tukey's test). *n* for 0.5 mM $CaCl_2$ = 7, 7, and 10 and for 2 mM $CaCl_2$ = 8, 7, and 5 recordings from four to nine larvae. (G) Cumulative probability histogram of miniature EJC amplitudes measured from *yw* controls and $shi^{12\text{-}12B}$; *shi-4C* incubated with FlAsH before illumination, during light inactivation and after FALI. *n* = 8, 5, 5, and 5 recordings from as many larvae. (H) Relative EJP amplitude measured during 10 min of 10-Hz stimulation in controls *yw* (*n* = 8 recordings from eight larvae) and in $shi^{12\text{-}12B}$; *shi-4C* loaded with FlAsH (*n* = 5 recordings from five larvae). Recordings were made by measuring EJPs for 2 min without illuminating the samples followed by 2 min of illumination to photoinactivate Dynamin. EJP amplitudes are plotted as the means of 30 s of recording and normalized to the means of the first 15 s per genotype. (inset) Example EJP data traces of *yw* and $shi^{12\text{-}12B}$; *shi-4C* (in black). Error bars show SEMs.

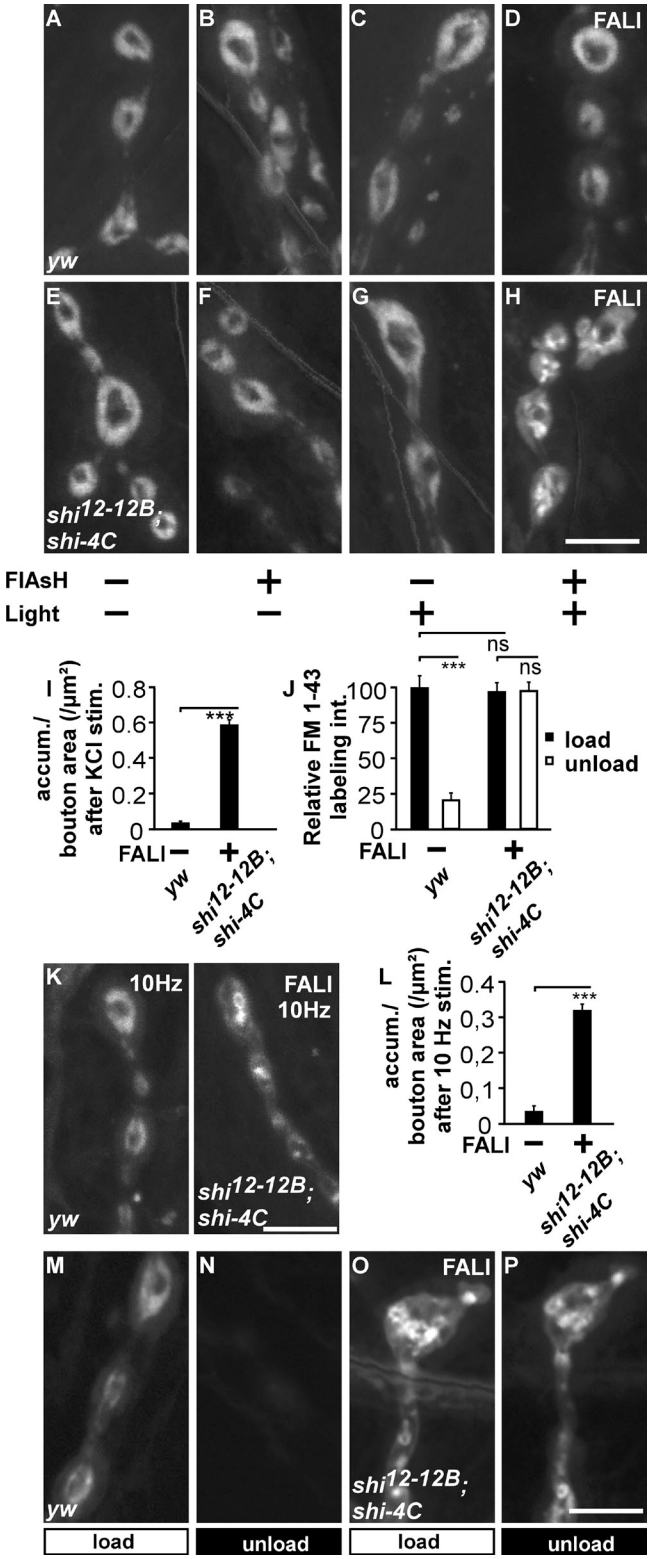

Figure 2. **Photoinactivation of Dynamin results in the formation of large membrane inclusions.** (A–H) FM 1-43 labeling in *yw* and *shi*$^{12\text{-}12B}$; *shi-4C* animals treated (+) or not treated (−) with FlAsH for 10 min and/or illumination for 2 min (±). All preparations were stimulated with KCl in the presence of FM 1-43 for 5 min. (I) Quantification of the number of FM 1-43–labeled membrane accumulations (accum.) per boutonic area in *yw* controls (n = 72 boutons from eight larvae) and in *shi*$^{12\text{-}12B}$; *shi-4C* after FALI (n = 72 boutons from 16 larvae). Error bars show SEMs; *t* test: ***, P < 0.0001. stim., stimulation. (J) Quantification of FM 1-43 labeling intensity (int.) after loading and unloading of *yw* controls (40 boutons from five larvae) and *yw; shi-4C* (n = 24 boutons from six larvae) after FALI normalized to the *yw* control (images shown in M–P). Error bars show SEMs. *t* test: ***, P < 0.0001. (K and L) FM 1-43 labeling (K) and quantification of the number of FM 1-43–labeled membrane accumulations per boutonic area (L) in *yw* (n = 32 boutons from five larvae) and *shi*$^{12\text{-}12B}$; *shi-4C* animals (n = 24 boutons from six larvae) after FALI when preparations were stimulated at 10 Hz for 5 min in the presence of FM 1-43. Error bars show SEMs. *t* test: ***, P < 0.0001. (M–P) Loading and unloading of FM 1-43 in *yw* and *shi*$^{12\text{-}12B}$; *shi-4C* after FALI. Preparations were loaded with FM 1-43 for 5 min in the presence of KCl (M and O, load) and unloaded using KCl stimulation for 10 min (N and P, unload; quantification in J). Bars, 5 µm.

shi^{ts1} at the restrictive temperature (Delgado et al., 2000; Verstreken et al., 2002). Under identical conditions, both *yw* controls or *shi*$^{12\text{-}12B}$; *shi-4C* animals, in which Dynamin was loaded with FlAsH but not inactivated by light, maintain neurotransmitter release well (Fig. 1 H, control). Hence, acute photoinactivation of Dynamin results in an inability to maintain neurotransmitter release during intense stimulation, consistent with a block in synaptic vesicle recycling.

Photoinactivation of Dynamin results in bulk membrane uptake

At a restrictive temperature, *shi*^{ts1} causes a block in synaptic membrane uptake during nerve stimulation (Koenig and Ikeda, 1989; Ramaswami et al., 1994; Delgado et al., 2000). To examine the effect of loss of Dynamin function on membrane uptake, we assessed FM 1-43 dye uptake during stimulation. FM 1-43 is a dye that binds to the membrane and becomes internalized into newly formed vesicles during nerve stimulation (Betz et al., 1996). We treated controls and *shi*$^{12\text{-}12B}$; *shi-4C* animals with or without FlAsH and with or without illumination for 2 min with 508-nm light and finally stimulated them using KCl in the presence of FM 1-43 (Fig. 2, A–H). In boutons of controls treated with or without FlAsH and with or without illumination, internalized FM 1-43 organizes in a typical doughnut-like pattern, indicating that FlAsH incubation or 508-nm light illumination do not measurably affect synaptic endocytosis (Fig. 2, A–D). Similarly, FM 1-43 dye, internalized in *shi*$^{12\text{-}12B}$; *shi-4C* larvae or in segments of such larvae in which Dynamin is not inactivated by FlAsH and light, distributes in a doughnut-like pattern (Fig. 2, E–G). Notably, in the segments in which Dynamin was photoinactivated by FALI, we observe clear membrane uptake (Fig. 2 H). The overall intensity of the internalized FM 1-43 in these areas is not different from controls (Fig. 2 J, black bars), but the dye distributes in large membranous structures (Fig. 2, H and I). This peculiar labeling pattern upon Dynamin inactivation is not the result of the KCl stimulation paradigm that was used, as we observe similar membrane internalization defects in Dynamin photoinactivated boutons that were electrically stimulated for 5 min at 10 Hz (Fig. 2, K and L). Hence, loss of Dynamin function results in uptake of bulk membrane, a phenotype that is very reminiscent of the defects observed upon photoinactivation of Chc or Clc (Heerssen et al., 2008; Kasprowicz et al., 2008) but at odds with the complete block in membrane uptake in *shi*^{ts1} at a restrictive temperature (Ramaswami et al., 1994; Delgado et al., 2000).

Next, to determine whether the defect in membrane uptake upon Dynamin photoinactivation correlates with a deficit to recycle the internalized membrane and release it in a new round of fusion, we first stimulated animals to load FM 1-43 into synaptic boutons in which Dynamin was photoinactivated and then, after a 10-min period of rest, stimulated the boutons a second time in the absence of dye, to assess unloading. In contrast to the efficient unloading of FM 1-43 observed in *yw* controls (Fig. 2, J, M, and N), in $shi^{12\text{-}12B}$; *shi-4C* boutons with photoinactivated Dynamin, the dye that was loaded in large membranous structures (Fig. 2, J and O) does not significantly unload (Fig. 2, J and P). Technical limitations preclude us from assessing very slow reformation of vesicles in the time frame of hours. Nonetheless, within the time frame of minutes, these data are in accordance with the acute inability to maintain neurotransmitter release during intense nerve stimulation and suggest that photoinactivation of Dynamin largely blocks synaptic vesicle recycling.

The specificity of Dynamin FlAsH-FALI

Photoactivation of FlAsH results in the production of singlet oxygen radicals that are less reactive than other radicals and specifically target methionines in a radius of 7–40 Å. This technology thus permits more selective inactivation of tagged proteins than some other forms of FALI (Yan et al., 2006). Nonetheless, the possibility remains that Dynamin-binding partners are (partially) inactivated in our study as well, thereby confounding the interpretation of the results. We therefore performed several tests as to assess the specificity of the Dynamin loss-of-function phenotype. First, we panneuronally expressed RNAi to *shi* in the nervous system (*dicer-2*/+; *shi* $RNAi^{v105971}$/+; *nSybGal4*/+). This tool results in a significant decrease in Dynamin immunofluorescence at synaptic boutons (Fig. 3, A–C). Expression of *shi* RNAi causes internalization of FM 1-43 in large membranous structures (Fig. 3, D–H), qualitatively reminiscent of the phenotype seen upon Dynamin photoinactivation. Second, we generated flies that express, at endogenous levels, tetracysteine-tagged EndoA (EndophilinA; Endo-4C; see Materials and methods; Fig. 3 I). EndoA is a Dynamin-binding partner, and the presence of Endo-4C rescues the lethality associated with *endoA*-null mutants ($endo^{1}$). Although controls internalize FM 1-43 dye efficiently (Fig. 3, J, K, and M), photoinactivation of EndoA-4C using FlAsH-FALI does not result in the appearance of large FM 1-43–labeled membrane structures, but it causes a significant reduction in dye uptake, similar to observations made in *endoA*-null mutants (Fig. 3, L and M; Verstreken et al., 2002). These results indicate that the defect in FM 1-43 dye distribution upon Dynamin photoinactivation is associated with loss of Dynamin function and that it is not a nonspecific effect of FlAsH-FALI.

Loss of Dynamin function induces bulk membrane internalization at the ultrastructural level

To further characterize the membrane inclusions formed upon stimulation of boutons during which Dynamin was photoinactivated, we performed transmission EM (TEM). We photoinactivated Dynamin in synaptic boutons of $shi^{12\text{-}12B}$; *shi-4C* using FALI, stimulated the samples, and imaged synaptic boutons. As a control, we also imaged boutons in which Dynamin was not photoinactivated. Similar to stimulated *yw* controls or to stimulated $shi^{12\text{-}12B}$; *shi-4C* without FALI or to shi^{ts1} mutants at permissive temperature, synaptic boutons in FlAsH-treated $shi^{12\text{-}12B}$; *shi-4C* in which Dynamin is not photoinactivated are filled with regular-sized synaptic vesicles (Fig. 4, A, B, I, M, and O). In contrast, stimulated synaptic boutons of $shi^{12\text{-}12B}$; *shi-4C* animals after photoinactivation of Dynamin show an accumulation of large membranous profiles (Fig. 4, C–H and K). In some images, we observe these profiles to be connected to the presynaptic membrane (Fig. 4, G and H). Additionally, synaptic terminals in which Dynamin was photoinactivated almost completely lack normal-sized synaptic vesicles (Fig. 4, I–K), and in sharp contrast to stimulated shi^{ts1} boutons kept at the restrictive temperature (Fig. 4, J–N [asterisks], P, and Q; Estes et al., 1996), they do not display the typical invaginated pits at their presynaptic membrane (Fig. 4, E, F, and L). Although the membrane internalization defects upon photoinactivation of Dynamin are substantial, other synaptic features, including mitochondrial number and active zone density, are not affected. Finally, we also observe similar membrane internalization defects in electron micrographs of boutons from stimulated *shi* RNAi–expressing animals, indicating that the defect is specific (Fig. S2, A–D). Hence, loss of Dynamin function results in qualitatively very different membrane uptake defects compared with the defects seen in shi^{ts1} mutants, and collectively, the data indicate that Dynamin prevents the uptake of large membranous cisternae upon stimulation.

Photoinactivation of Dynamin blocks Clathrin and α-Ada recruitment upon stimulation

Loss of Dynamin function results in the internalization of large membranous structures that appear very similar to those seen upon loss of Chc or Clc function (Heerssen et al., 2008; Kasprowicz et al., 2008). We therefore hypothesized that in neurons, in addition to membrane fission, Dynamin would also be required to coordinate Clathrin-dependent steps in the formation of synaptic vesicles. To address this question, we used superresolution microscopy and assessed Chc and α-Ada localization before and after stimulation of synaptic boutons. Immunohistochemistry using anti-Chc antibodies is difficult in *Drosophila* larvae, and overexpression of a Clc-GFP fusion causes strong morphological defects at the larval NMJ. We therefore used yeast recombination and phiC-31–mediated genomic integration to express HA-Chc at endogenous levels. The presence of this construct rescues the lethality associated with chc^{1}-null mutants (Bazinet et al., 1993; Kasprowicz et al., 2008). Additionally, anti-HA labeling of larval fillets that express HA-Chc shows clear presynaptic boutonic labeling that is absent in *yw* controls (presynaptic boutonic anti-HA intensity in *yw* is 2.8 ± 0.3 arbitrary units [a.u.] and in *yw*; *HA-Chc*/+ is 63.2 ± 4.2 a.u.; *t* test: $P < 0.0001$), indicating that the tagged protein is expressed and functional.

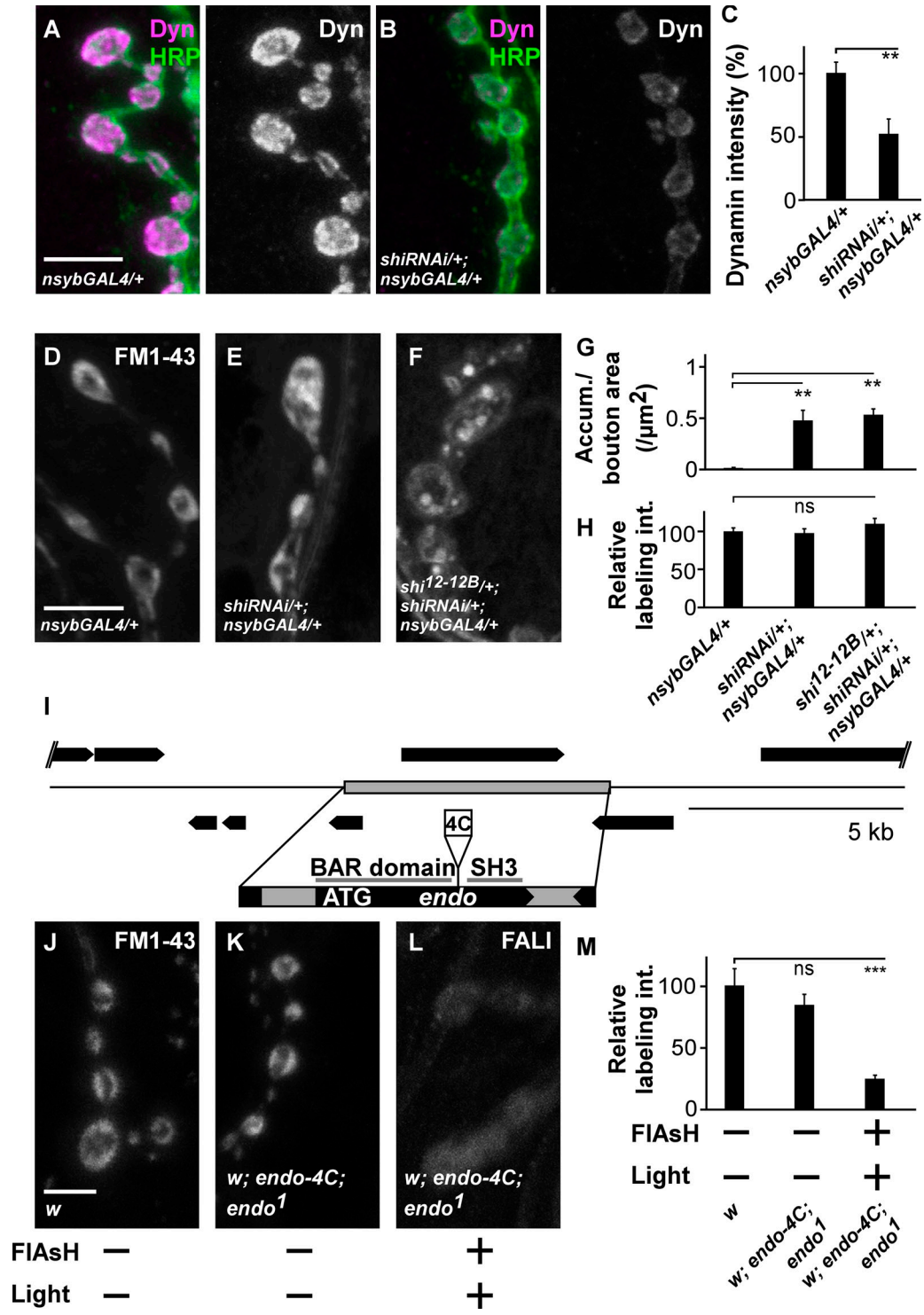

Figure 3. **Dynamin FlAsH-FALI is specific.** (A–C) Labeling of controls (*dicer-2/+;; nSybGal4/+*; A) and larvae expressing *shi* RNAi (*dicer-2/+; shi RNAi/+; nSybGal4/+*; B) third instar larval boutons with anti-Dynamin (Dyn) and anti-HRP and quantification of boutonic anti-Dynamin labeling intensity. Error bars show SEMs; *t* test: **, P < 0.001 (*n* = 10 NMJs from five larvae per genotype). (D–F) FM 1-43 dye uptake measured after 5 min of stimulation with KCl in controls (*dicer-2/+;; nSybGal4/+*; D), larvae expressing RNAi to *shi* (*dicer-2/+; shi RNAi/+; nSybGal4/+*; E) and in heterozygous mutant *shi* larvae that express RNAi to *shi* (*shi*$^{12\text{-}12B}$*/dicer-2; shi RNAi/+; nsybGAL4/+*; F). (G and H) Quantification of the number of FM 1-43–labeled accumulations (Accum.) per boutonic area (G) and relative FM 1-43 labeling intensity (int.; H) in controls (*dicer-2/+;; nSybGal4/+*), in larvae expressing RNAi to *shi* (*dicer-2/+; shi RNAi/+; nSybGal4/+*), and in heterozygous mutant *shi* larvae that express RNAi to *shi* (*shi*$^{12\text{-}12B}$*/dicer-2; shi RNAi/+; nsybGAL4/+*). Error bars show SEMs; ANOVA (post hoc Tukey's test): **, P < 0.001. In G, *n* = 24, 36, and 60 boutons from three, seven, and five animals. In H, *n* = 24, 36, and 20 boutons from three, five, and four animals. (I) Strategy used to generate a genomic Endo-4C construct. The 4C is inserted between the BAR and SH3 domain. ATG is the start codon. (J–L) FM 1-43 labeling in *w* and *w; endo-4C; endo*^{1} animals treated (+) or not treated (−) with FlAsH for 10 min and/or illumination for 5 min (±). All preparations were stimulated with KCl in the presence of FM 1-43 for 1 min, washed, and imaged. (M) Quantification of FM 1-43 labeling intensity after loading of *w* and *w; endo-4C; endo*^{1} before and after FALI normalized to the *w* control. Error bars show SEMs; ANOVA (post hoc Tukey's test): ***, P < 0.0001. *n* = 24, 60, and 64 boutons from six, four, and seven animals. Bars, 5 µm.

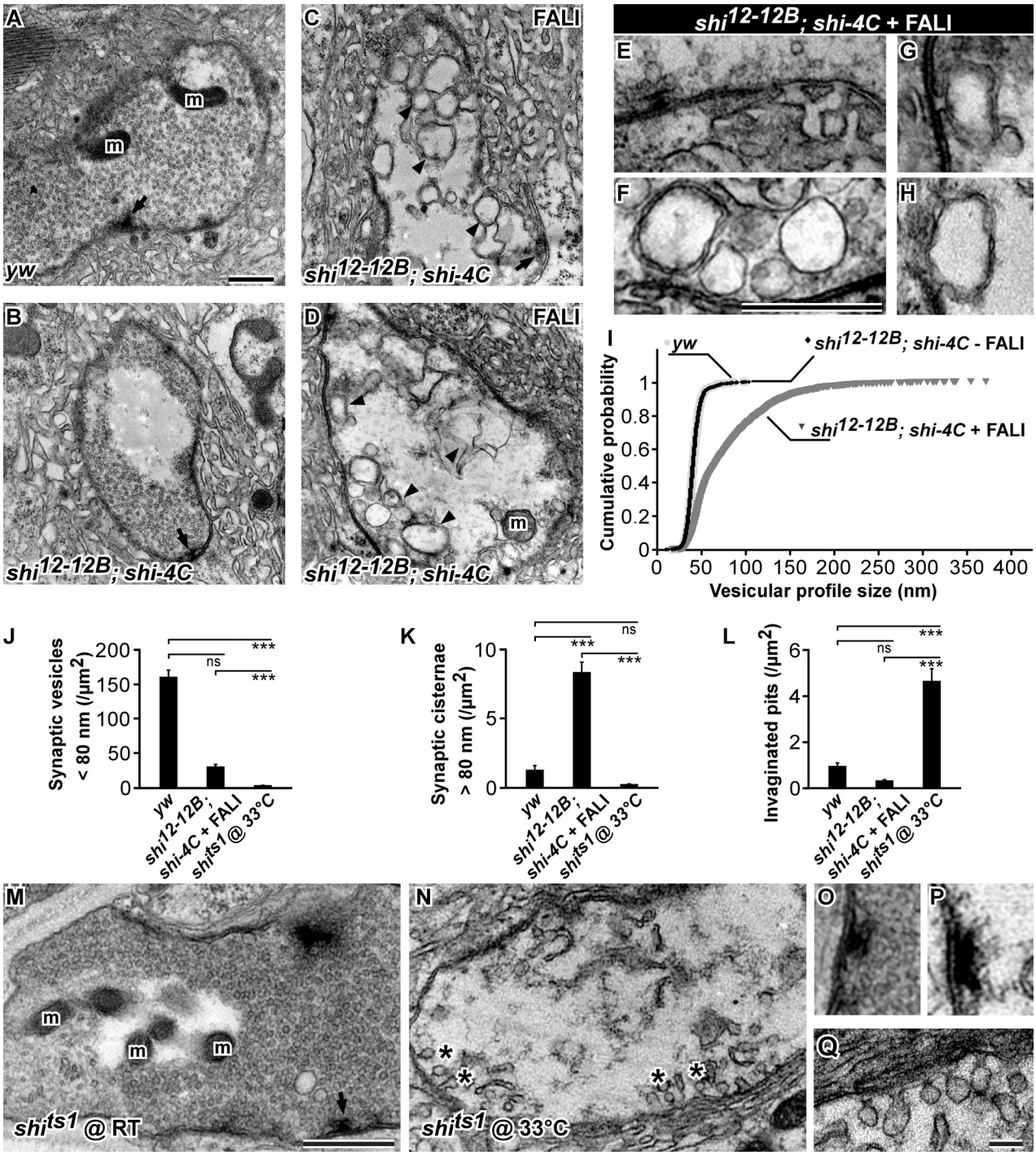

Figure 4. **Photoinactivation of Dynamin results in massive bulk membrane uptake, whereas *shi^{ts1}* mutant boutons at restrictive temperature show an accumulation of invaginated pits.** (A and B) Electron micrographs of *yw* (A) and *shi$^{12\text{-}12B}$; shi-4C* (B) control boutons stimulated for 5 min with KCl without FALI. Arrows, T bar; m, mitochondria. (C–H) Electron micrographs of *shi$^{12\text{-}12B}$; shi-4C* boutons in which Dynamin was photoinactivated using FALI and subsequently stimulated for 5 min with KCl. High magnifications of the membrane with an active zone decorated with a T bar (E) and of inner membrane inclusions (F–H). Arrowheads, submembrane; arrow, T bar; m, mitochondria. (I) Cumulative probability distributions of vesicular profile diameter size in *yw* (n = 1,291 vesicles from three larvae), *shi$^{12\text{-}12B}$; shi-4C* controls not treated with FALI (n = 1,291 vesicles from three larvae), and *shi$^{12\text{-}12B}$; shi-4C* treated with FALI (n = 2,824 vesicles from three larvae). (J–L) Quantification of different boutonic features: the number of synaptic vesicles with a diameter <80 nm per area (J), the number of synaptic vesicles with a diameter >80 nm per area (K), and the number of invaginated pits per area (L) in *yw* controls (n = 33 bouton profiles from three larvae), *shi$^{12\text{-}12B}$; shi-4C* after FALI (n = 27 bouton profiles from three larvae), and *shi^{ts1}* at a restrictive temperature (33°C; n = 16 profiles from three larvae). Error bars show SEMs; ANOVA (post hoc Tukey's test): ***, P < 0.0001. (M and N) Electron micrographs of *shi^{ts1}* boutons stimulated for 5 min with KCl at permissive (25°C; M) and restrictive (33°C) temperature (N). Asterisks, invaginated pits; arrow, T bar; m, mitochondria. (O–Q) Higher magnification of the active zones in *shi^{ts1}* boutons stimulated for 5 min with KCl at permissive (O) and restrictive temperature (P) and of invaginated pits in *shi^{ts1}* boutons at restrictive temperature (Q). Note the lack of synaptic vesicles around the active zone in *shi^{ts1}* at restrictive temperature. Bars: (A–H, M, and N) 0.5 µm; (O–Q) 0.1 µm.

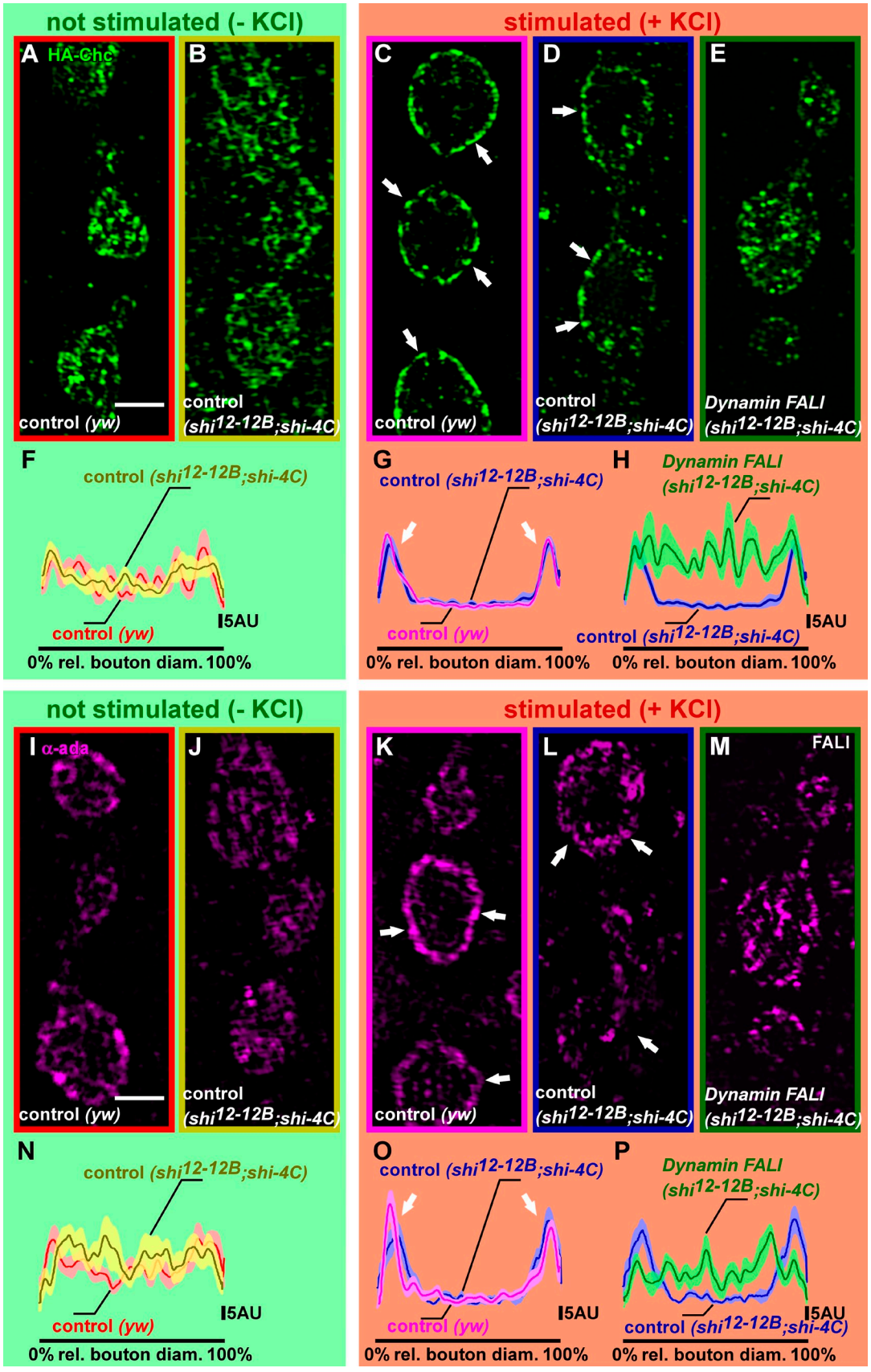

Figure 5. **Stimulus-dependent Chc and α-Ada recruitments are blocked upon Dynamin photoinactivation.** (A–H) Superresolution imaging of HA-Chc fusion proteins with anti-HA antibodies, using structured illumination microscopy in not stimulated (−KCl) and stimulated (+KCl; 90 mM for 5 min) preparations. (A and B) Labeling of *yw; HA-chc* controls (*yw*) and *shi*$^{12\text{-}12B}$*/Y; HA-chc/shi-4C* without FALI at rest (−KCl). Note the presence of Chc in the bouton center

Next, we assessed boutonic HA-Chc localization before and after neuronal stimulation in controls and in boutons in which Dynamin was photoinactivated. In nonstimulated control boutons or boutons in which Dynamin is not photoinactivated, HA-Chc is widely distributed (Fig. 5, A, B, and F; and Fig. S3, A and B; see also Materials and methods). However after stimulation, the protein relocalizes and concentrates at the bouton periphery at the expense of its localization in the bouton center (Fig. 5, C, D, and G; and Fig. S3, C and D). In contrast, photoinactivation of Dynamin blocks this activity-dependent relocalization of HA-Chc, and despite the neuronal stimulation, the protein remains distributed throughout the bouton (Fig. 5, E and H; and Fig. S3 E). Attesting to the specificity of this phenotype, boutons in which Dynamin was knocked down using RNAi display qualitatively very similar phenotypes (Fig. S4, A–C). Hence, the data suggest that Dynamin is needed to coordinate Clathrin-dependent steps during the formation of synaptic vesicles.

The AP2 complex, which connects the Clathrin lattice to the membrane, acts as a hub during vesicle formation in nonneuronal cells (Puthenveedu and von Zastrow, 2006; Loerke et al., 2009; Mettlen et al., 2009; Aguet et al., 2013). We therefore also examined the localization of α-Ada before and after stimulation in controls and at synapses in which Dynamin was photoinactivated. Similar to *HA-chc* localization, we found that α-Ada becomes more concentrated in the bouton periphery upon neuronal stimulation of controls, and this effect is lost at NMJs in which Dynamin was photoinactivated (Fig. 5, I–P; and Fig. S3, F–J). Similarly, we observe a comparable phenotype upon RNAi-mediated knockdown of Dynamin (Fig. S4, D–F). Hence, the data suggest that Dynamin coordinates vesicle budding by stabilizing or recruiting α-Ada and Chc at the membrane.

Stimulus-dependent Clathrin and α-Ada recruitment in *shi^{ts1}* mutants

Given that photoinactivation of Dynamin causes massive membrane internalization, whereas shifting *shi^{ts1}* to a restrictive temperature blocks membrane uptake, we wondered whether HA-Chc and α-Ada still relocalize to the bouton periphery in *shi^{ts1}* mutants at a restrictive temperature upon stimulation. We therefore expressed HA-Chc in *shi^{ts1}* and stimulated the larval fillets at permissive (22°C) or at restrictive temperature (33°C). Anti-HA labeling and anti–α-Ada labeling in stimulated *shi^{ts1}* at 33°C show HA-Chc and α-Ada labeling concentrating in the bouton periphery (Fig. 6, A and B). This labeling of HA-Chc and α-Ada in *shi^{ts1}* at 33°C is different from the block in HA-Chc and α-Ada relocalization upon photoinactivation of Dynamin (Fig. 5), but it is less pronounced than the relocalization seen in control animals or in *shi^{ts1}* animals at permissive temperature (Fig. 5 and Fig. 6, A and B). This difference may be caused by the formation of the deeply invaginated pits in *shi^{ts1}* that may result in a "broader rim" of Clathrin and α-Ada at the membrane. Nonetheless, our data indicate that *shi^{ts1}* at restrictive temperature retains, at least in part, the ability to facilitate Clathrin and α-Ada relocalization upon stimulation, a function that is lost upon photoinactivation of Dynamin.

Our data are consistent with a model in which, in *shi^{ts1}* at restrictive temperature, Dynamin is trapped in a metastable, aggregated state, at the neck of nascent vesicles (Chen et al., 2002). In this capacity, Dynamin would still support Clathrin-dependent endocytic functions that prevent bulk membrane uptake while having lost its activity to mediate GTP-dependent membrane fission. To test this model, we photoinactivated Dynamin in *shi^{ts1}* mutants and assessed membrane internalization. We therefore generated *shi^{ts1}* flies that also express Shi-4C (*shi^{ts1}/Y*; *shi-4C/+*). Given that Dynamin forms multimeric complexes and based on quantification of the intensity of boutonic labeling using anti-Dynamin antibodies in *shi^{ts1}/Y* (258.7 ± 4.7 a.u.) and in *shi^{ts1}/Y*; *shi-4C/+* larvae (401.8 ± 46.3 a.u.; *t* test: $P < 0.05$), we estimate that for every two Shi^{ts1} molecules, about one Shi-4C is expressed in *shi^{ts1}/Y*; *shi-4C/+* animals (Fig. 6 C). Hence, assuming similar incorporation of these two types of Dynamin in Dynamin multimers, virtually every Dynamin multimeric complex harbors both types of Dynamin (for multimers without Shi-4C, $P = 3.01 \times 10^{-5}$; for multimers without Shi^{ts1}, $P = 3.03 \times 10^{-13}$; Fig. 6 C). Given that both Shi^{ts1} and Shi-4C act dominantly (Fig. S5, A–C; Kitamoto, 2001), such that even when wild-type Dynamin is present they result in strong membrane uptake defects (see following paragraph), Shi^{ts1} can first be trapped in a metastable state at restrictive temperature. In a second phase, using FALI, photoinactivation of Shi-4C can then be used to also acutely photoinactivate Shi^{ts1}–Shi-4C complexes.

We stimulated *shi^{ts1}/Y*; *shi-4C/+* animals at the restrictive temperature (33°C) without photoinactivating Dynamin and tested for endocytosis defects using FM 1-43. This condition results in a block in membrane uptake (Fig. 6, E and H) as compared with control (*shi^{ts1}/Y*; *shi-4C/+*) at 22°C (Fig. 6 D), indicating Shi^{ts1} can indeed inhibit membrane uptake in a dominant fashion. Next, we tested for membrane uptake in stimulated *shi^{ts1}/Y*; *shi-4C/+* animals in which we photoinactivated Dynamin using FALI at the permissive temperature. Here, we find that FM 1-43 concentrates in large inclusions (Fig. 6 G), indicating that also

and at the bouton periphery as quantified in F (n = 10 boutons from three larvae); see Materials and methods and also Fig. S3. rel., relative. (C–E) Labeling of *yw*; *HA-chc* (*yw*) and *shi$^{12\text{-}12B}$/Y*; *HA-chc/shi-4C*, stimulated with KCl without Dynamin inactivation (blue; C and D) and with Dynamin inactivation using FALI (E). Note that in the stimulated controls (C and D), Chc becomes more concentrated in the bouton periphery than in animals in which Dynamin was inactivated (E) as quantified in G and H (n = 11–12 boutons from four to five larvae); see Materials and methods and also Fig. S3. (I–P) Superresolution imaging of α-Ada using structured illumination microscopy in not stimulated (−KCl) and stimulated (+KCl; 90 mM for 5 min) preparations. (I and J) Labeling of *yw* controls (*yw*) and *shi$^{12\text{-}12B}$/Y*; *shi-4C/+* without FALI at rest (−KCl). Note the presence of α-Ada in the bouton center and at the bouton periphery as quantified in N (n = 9–10 boutons from three to four larvae); see Materials and methods and also Fig. S3. (K–M) Labeling of *yw* (*yw*) and *shi$^{12\text{-}12B}$/Y*; *shi-4C/+*, stimulated with KCl without Dynamin inactivation (blue; K and L) and with Dynamin inactivation using FALI (M). Note that in the stimulated controls (K and L), α-Ada becomes more concentrated in the bouton periphery than in animals in which Dynamin was inactivated (M) as quantified in O and P (n = 9–10 boutons from four to five larvae); see Materials and methods and also Fig. S3. SEM is shown in the lighter shade. Arrows, plasma membrane. Bars, 2 µm.

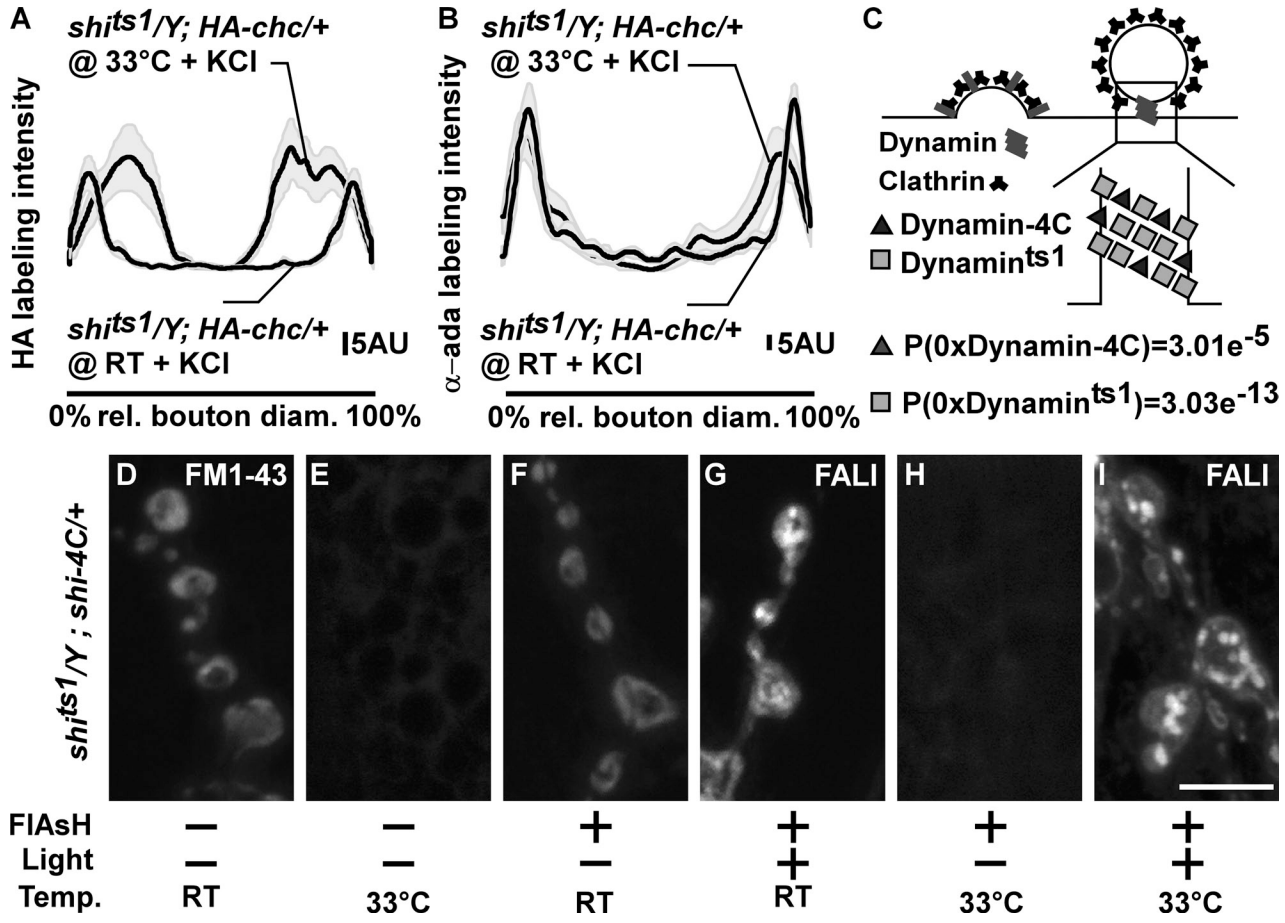

Figure 6. **Photoinactivation of Dynamin converts invaginated pits in *shi*^{ts1} mutants into bulk cisternae.** (A and B) Quantification of the HA-Chc (A, *n* = 11 boutons from seven larvae each) and α-Ada (B, *n* = 7–10 boutons from six to seven larvae) labeling intensity in a line over the (largest) bouton diameter (and normalized to the length of the bouton diameter; see Materials and methods) in KCl-stimulated *shi*^{ts1}*/Y; HA-chc/+* at permissive (RT) temperature and *shi*^{ts1}*/Y; HA-chc/+* at restrictive temperature (33°C); see Materials and methods. Averages are in black lines, and SEMs are in gray shades. rel., relative. (C) Model of the distribution of different Dynamin molecules (Shi-4C and Shi^{ts1}) in endocytic pits (based on anti-Dynamin labeling intensity—see Stimulus-dependent Clathrin and α-Ada recruitment in shi^{ts1} mutants in the Results section) and calculation of the probability that Dynamin rings consist only of Shi^{ts1} or only of Shi-4C in *shi*^{ts1}*/Y; shi-4C/+* larvae. (D–I) FM 1-43 labeling in *shi*^{ts1}*/Y; shi-4C/+* larvae treated (+; F–I) or not treated (−; D and E) with FlAsH for 10 min and illuminated for 2 min (+; G and I) at permissive (D, F, and G) or restrictive (E, H, and I) temperature. All preparations were stimulated for 5 min with KCl in the presence of FM 1-43. Note that *shi*^{ts1}*/Y; shi-4C/+* animals at restrictive temperature without FALI phenocopy *shi*^{ts1} animals and do not internalize FM 1-43, whereas *shi*^{ts1}*/Y; shi-4C/+* animals at restrictive temperature after FALI also internalize FM 1-43 in cisternal inclusions, similar to *shi*$^{12\text{-}12B}$*; shi-4C* animals in which Dynamin was photoinactivated. Bar, 5 µm.

Shi-4C acts dominantly (Fig. S5). Finally, we kept FlAsH-treated *shi*^{ts1}*/Y*; *shi-4C/+* animals at 33°C to trap Shi^{ts1} in a metastable state followed by photoinactivation of Shi-4C and then assessed FM 1-43 dye uptake upon stimulation. Despite the fact that Shi^{ts1} is kept at a restrictive temperature, illustrated by the undetectable FM 1-43 internalization outside of the illuminated area (Fig. 6 H), boutons within the illuminated area, in which Shi-4C was photoinactivated, now show FM 1-43–labeled membrane inclusions (Fig. 6 I). Hence, our data suggest that Dynamin in *shi*^{ts1} retains the ability to prevent bulk membrane retrieval, but when inactivated, bulk cisternae formation ensues.

Stimulation of *shi*^{ts1} mutant synapses causes the formation of deeply invaginated pits (Fig. 4, L, N, and Q). We therefore investigated the membrane inclusions formed upon photoinactivation of Dynamin in *shi*^{ts1} boutons using TEM on stimulated *shi*^{ts1}*/Y*; *shi-4C/+* boutons in different conditions. Boutons of *shi*^{ts1}*/Y*; *shi-4C/+* animals stimulated at 22°C are abundantly packed with synaptic vesicles (Fig. 7, A and G), similar to *yw* controls (Fig. 4 A). Conversely, boutons of stimulated *shi*^{ts1}*/Y*; *shi-4C/+* animals at restrictive temperature show numerous deeply invaginated pits, and they are almost devoid of synaptic vesicles (Fig. 7, B, G, and I). Interestingly, when Dynamin is photoinactivated in the same *shi*^{ts1}*/Y*; *shi-4C/+* animals kept at restrictive temperature, the boutons do not display an accumulation of invaginated pits upon stimulation (Fig. 7, C, D, and I), instead these boutons harbor massive membrane cisternae that are sometimes intertwined and double invaginated, appearing as double membranes (Fig. 7, C, D, G, and H), similar to *shi*$^{12\text{-}12B}$; *shi-4C* with photoinactivated Dynamin (see previous section; Fig. 4, C–H). To further assess whether the presynaptic membrane surface or the membrane surface of these cisternal structures contain invaginated pits, we also performed 3D electron tomography on thick 300-nm sections (Fig. 7, E and F; and Video 1). Inspection of the plasma membrane surface does not reveal invaginated pits (Fig. 7 E), and reconstructions of individual cisternal structures (Fig. 7 F) show

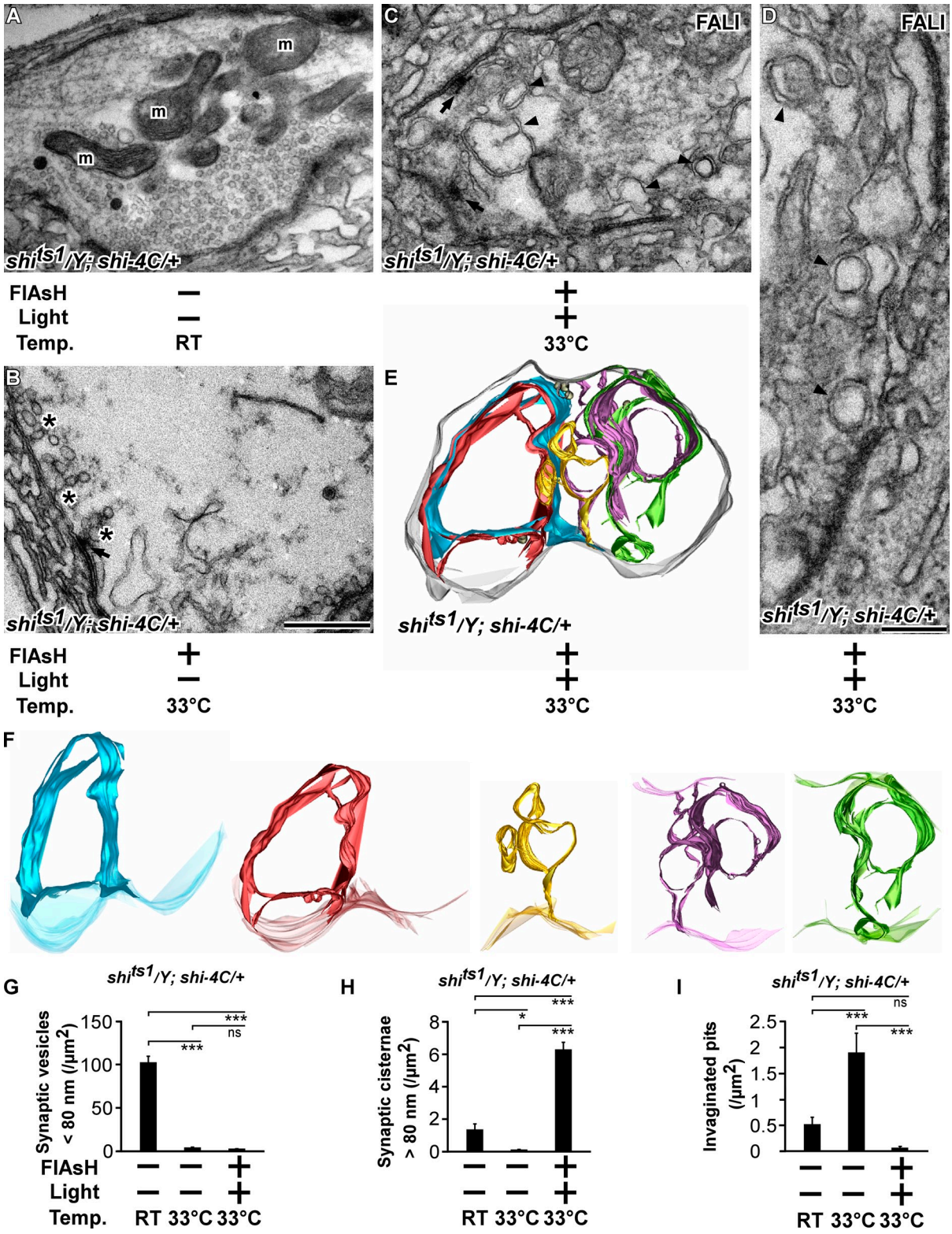

Figure 7. **Invaginated pits in *shi^{ts1}* mutants are converted into bulk cisternae upon Dynamin photoinactivation at the ultrastructural level.** (A–D) Electron micrographs of *shi^{ts1}/Y; shi-4C* larvae treated with FlAsH for 10 min (+; B–D) or not treated (−; A) and illuminated for 2 min (+; C and D) or not illuminated (−; A and B) at permissive (RT; A) or restrictive (33°C) temperature (B–D) stimulated for 5 min with KCl. Bars: (A–C) 0.5 µm; (D) 0.25 µm. Arrowheads, submembrane inclusions; arrows, T bar; m, mitochondria; asterisks, invaginated pits. (E and F) Model of a bouton after surface rendering of a tomogram of *shi^{ts1}/Y; shi-4C* larvae after FALI (+/+) at restrictive temperature 33°C stimulated for 5 min with KCl (see also Video 1). (E) Note that some of the membrane inclusions are so massive that they are intertwined and folded inside each other. (F) Individual tomography models of different membrane inclusions. Gray, plasma membrane; blue, red, yellow, purple, and green, membrane inclusions. (G–I) Quantification of the number of synaptic vesicles <80 nm per area (G), the number of synaptic cisternae >80 nm per area (H), and the number of invaginated pits per area (I) in *shi^{ts1}/Y; shi-4C* larvae at 22°C (RT) not treated with FALI (−/−), at 33°C not treated with FALI (−/−), and at 33°C after FALI (+/+). Error bars show SEMs; ANOVA (post hoc Tukey's test): *, $P < 0.01$; ***, $P < 0.0001$. $n = 13$, 10, and 14 bouton profiles from three larvae each.

that they are connected to the plasma membrane but also do not contain a significant number of invaginated pits (Fig. 7, F and I). Collectively, these data suggest that Shi^{ts1} retains specific aspects of Dynamin function involved in coordinating Clathrin-dependent steps that prevent bulk membrane retrieval while blocking membrane fission.

Discussion

Dynamin is one of the best-studied endocytic proteins, but the effect of acute, complete, or very strong Dynamin inactivation in the absence of developmental effects in neurons has not been reported (Koenig and Ikeda, 1989; Merrifield et al., 2002; Macia et al., 2006; Ferguson et al., 2007; Raimondi et al., 2011). The available data based on biochemistry, genetics, and pharmacology indicate an essential function for Dynamin in the fission of vesicles from the plasma membrane. Here, we provide evidence that during synaptic vesicle formation, Dynamin is critically needed to also coordinate the recruitment of Clathrin and AP2, factors needed for vesicle budding. Previous data already indicated that Clathrin prevents bulk endosome-like structure formation (Heerssen et al., 2008; Kasprowicz et al., 2008), and a role for Clathrin adaptors in preventing bulk cisternae retrieval is also consistent with the observation that mutations in such adaptors increase the incidence of detecting cisternal-like structures in different species (González-Gaitán and Jäckle, 1997; Zhang et al., 1998; Nonet et al., 1999; Gu et al., 2013). Hence, our data suggest that by stabilizing Clathrin- and AP2-dependent events, Dynamin takes on a critical role during synaptic vesicle biogenesis. Recent work in nonneuronal systems links a role for Dynamin in controlling actin polymerization (Ferguson et al., 2009), but it is currently not known whether this function relates to the role for Dynamin in facilitating Clathrin recruitment at synapses. Dynamin (and Clathrin) also appears important for the formation of synaptic vesicles from the membranes that were retrieved by bulk endocytosis. Without excluding slow Dynamin- or Clathrin-independent vesicle formation mechanisms that operate at time frames much longer than the 10 min we tested, we find that the photoinactivation of Dynamin at the NMJ very severely blocks synaptic vesicle recycling as gauged by a block in FM 1-43 unloading, and it also results in an inability to maintain neurotransmitter release during intense stimulation. Hence, efficient synaptic vesicle recycling requires Dynamin.

Our work also leads us to conclude that Dynamin is dispensable for bulk membrane retrieval in neurons. This conclusion contradicts earlier studies that indicated a phosphorylation-dependent role of Dynamin in bulk membrane uptake (Evans and Cousin, 2007; Clayton et al., 2009, 2010; Wu et al., 2009; Smillie and Cousin, 2012). In this model, Calcineurin-dependent dephosphorylation of Dynamin controls the interaction with Syndapin, which was shown to facilitate bulk cisternae formation (Anggono et al., 2006; Clayton et al., 2009). These inconsistencies may be the result of the difference in preparations used. We used a live preparation and different genetic methodologies that were thoroughly tested for specificity, to inactivate Dynamin function, all yielding consistent results. Likewise, also in cultured *dynamin* mutant nonneuronal mouse cells, the formation of bulk cisternae is apparent (Park et al., 2013). Hence, the data indicate that bulk cisternae form more readily in the absence rather than the presence of Dynamin. Consistent with this conclusion, in stimulated fly *dap160* mutants, in which Dynamin mislocalizes, larger vesicles and cisternae are also apparent (Marie et al., 2004; Verstreken et al., 2005; Winther et al., 2013).

A role for Dynamin in preventing bulk membrane retrieval at synapses seems to be at odds with the accumulation of invaginated pits in *shi^{ts1}* mutants or in neurons in which Dynamin was inhibited by pharmacological means (Macia et al., 2006; Newton et al., 2006). However, in all these conditions, some Dynamin function almost certainly remained or Dynamin may have been trapped in a metastable state. First, triple *dynamin* mouse knockout neurons have not yet been generated, and *dynamin*-null mutant fruit flies die early during development. In nonneuronal triple knockout fibroblasts, the loss of *dynamin* does cause bulk membrane retrieval (Park et al., 2013), but it remains to be seen whether the molecular mechanisms of stimulus-dependent bulk membrane uptake in neurons compares with bulk retrieval in fibroblasts. Second, drugs used to inhibit Dynamin function have been reported to be not entirely specific (Park et al., 2013). Off-target effects or incomplete inhibition of all the functions of Dynamin may complicate the interpretation of the data. Finally, the temperature-sensitive Shi^{ts1} protein that in a dominant fashion causes the buildup of invaginated pits at restrictive temperature appears to be locked in a metastable state visible by TEM. This mutant Dynamin protein may still harbor some function. Consistent with this idea, we show that when we photoinactivate Dynamin and Dynamin complexes that consist of both Shi-4C and Shi^{ts1} at restrictive temperature, invaginated pits are lost, and massive bulk cisternae formation ensues. This phenotype is very reminiscent of that seen upon photoinactivation of Dynamin itself, suggesting that despite blocking membrane recycling, the Shi^{ts1} protein retained some functionality in that it prevents bulk membrane retrieval. Hence, strong inhibition of Dynamin function reveals a critical role for the protein in preventing the formation of bulk cisternae. We believe this mechanism may turn out to be evolutionarily conserved because heavily stimulated mouse *dynamin1* knockout neurons also show bulk endosome-like structures; however, here, the formation of invaginated pits was not entirely restricted (Hayashi et al., 2008), a feature potentially caused by the presence of the other Dynamin isoforms.

Although Dynamin is essential for membrane fission, our work now suggests that the protein also serves an essential role in stabilizing synaptic endocytic complexes that involve Clathrin and AP2. This notion is consistent with the emerging role for Dynamin in nonneuronal cells during the early steps of Clathrin-coated pit formation (Conner and Schmid, 2003; Loerke et al., 2009; Mettlen et al., 2009). Studies of Dynamin in cell culture, in which GTPase domain mutants were overexpressed, suggested a role for the protein in Clathrin-coated pit formation (Damke et al., 2001). Moreover, in vitro imaging experiments revealed that the level of Dynamin2 at new Clathrin-coated pits negatively correlates with the lifetime of a pit, further suggesting that the maturation of a nascent bud depends on Dynamin2 in these cells (Aguet et al., 2013). In neurons, Dynamin directly interacts with several synaptic endocytic factors that, at least in part, may act during

earlier phases of endocytosis as well, including Dap160/Intersectin, Syndapin, and Amphiphysin (David et al., 1996; Okamoto et al., 1997; Qualmann et al., 1999; Simpson et al., 1999; Koh et al., 2004; Ferguson et al., 2009; Winther et al., 2013). Also before fission, another Dynamin-binding partner, EndoA, has been shown to localize to the neck of deeply invaginated pits in a Dynamin-dependent manner, suggesting it aids in the Dynamin-catalyzed fission reaction (Sundborger et al., 2011). Hence, it is tempting to speculate that Dynamin's involvement at synapses is needed for proper endocytic complex assembly at different stages of vesicle formation. We now find that during the first steps of synaptic vesicle formation, Dynamin would stabilize AP2, culminating in Clathrin polymerization and cage formation, a process that prevents the retrieval of bulk endosomes and facilitates the formation of uniformly sized synaptic vesicles.

Materials and methods

Genetics and behavior tests

Fly stocks were maintained on standard maize meal and molasses medium. Mutant and RNAi stocks were obtained from the Bloomington Drosophila Stock Center and from the Vienna Drosophila RNAi Center or were gifts. $shi^{12\text{-}12B}$ is a *shi*-null mutant and was generated by C. Poodry (University of California, Santa Cruz, Santa Cruz, CA) by γ rays, resulting in genomic rearrangements (Grant et al., 1998). $shi^{12\text{-}12B}$ flies were given to us by M. Ramaswami (Trinity College, Dublin, Ireland). shi^{ts1} harbors a G273D mutation (Chen et al., 2002). The upstream activation sequence–*shi* RNAi is *v105971* obtained from the Vienna Drosophila RNAi Center, $endo^{1}$ is an *endoA*-null allele that corresponds to P[EP]927 outcrossed to w^{1118} for several generations (Verstreken et al., 2002), and chc^{1} is a *chc*-null mutant (Bazinet et al., 1993). Transgenes are described in the Molecular biology section of the Materials and methods. To collect third instar larvae for FlAsH-FALI, embryos were raised on black currant plates with fresh yeast paste; for RNAi expression, flies were crossed on standard medium, at RT for 3 d, and then shifted to 25°C. Third instar larvae were directly collected from the vials.

The flight and negative geotaxis assays were performed using batches of five flies. For the flight assay, flies were placed in an empty vial and tapped down. Flies able to fly were scored as 1, whereas those that did not were scored as 0. Negative geotaxis tests were also performed using batches of five flies. Flies were tapped down in an empty vial, and the number of flies that crossed a 4 cm mark within 5 s was counted.

Molecular biology

The *shi-4C* construct was generated by retrieving the genomic region of the *shi* gene (*CG18102*) and the nearby 5′-located gene (*CG15916*) using *E. coli* recombination from BACR32K23 with primers listed in Table S1 (Venken et al., 2006, 2008). A FLAG-4C tag (a peptide fusion of FLAG and an optimized FlAsH-binding tetracysteine tag; Martin et al., 2005) was added at the beginning of the middle domain of the *shi* gene by recombineering-mediated tagging (Venken et al., 2006, 2008). The *endo-4C* construct was generated using recombination in *Saccharomyces cerevisiae*. Two overlapping PCR fragments that encompass *endoA* and incorporate a 4C tag (without FLAG) in between the BAR (Bin1/amphiphysin/Rvs167) and SH3 domain and that harbor homology arms to *pFL44sw⁺AttB* (Khuong et al., 2013) were prepared using the primers listed in Table S1. *pFL44sw⁺AttB* was cut with BamH1, and the primers and plasmid were combined using yeast recombination (Merhi et al., 2011). To generate *HA-chc*, the genomic region of the *chc* gene (*CG9012*) and the nearby 5′-located gene *CG32582* were first retrieved by *E. coli* recombination from BACR25C18 into the *attB*-P[acman]-Amp-R vector (Venken et al., 2006), adapted for *S. cerevisiae*, using two homology arms. Next, this plasmid was cut with BsiWI and BbVcI, and the HA tag was incorporated at the N terminus of the *chc* gene by yeast recombination of overlapping PCR fragments that contain the HA tag. The primers used to generate the homology arms and the overlapping PCR fragments with the HA tag are listed in Table S1. Recombined constructs were sequenced, and transgenic animals were generated using phiC-31–mediated integration in *PBac{yellow[+]-attP-3B}VK00033* for *shi-4C* and y^{1} w^{67c23}; P{CaryP}attP40 for *Endo-4C* and for *HA-chc*.

Photoinactivation of Shi-4C and Endo-4C and visualization of FlAsH fluorescence

To load the 4C tag with FlAsH (Invitrogen), third instar larvae were dissected in HL-3 (110 mM NaCl, 5 mM KCl, 10 mM $NaHCO_3$, 5 mM Hepes, 30 mM sucrose, 5 mM trehalose, and 10 mM $MgCl_2$, pH 7.2; Stewart et al., 1994) and incubated for 10 min in 1 µM FlAsH in the dark. Subsequently, preparations were washed in Bal (Invitrogen) to remove unbound FlAsH and three times with HL-3. Photoinactivation of Dynamin or EndoA was performed on synapses in segments A3 or A4 by illuminating the NMJs in a hemisegment with epifluorescent 500 ± 12 nm (Intensilight C-HGFI; Nikon) band pass–filtered light (excitation filter, 500/24 nm; dichroic mirror, 520 nm) for 2 min (Dynamin) or 5 min (EndoA) using a 40×, 0.8 NA water immersion objective on a microscope (Eclipse F1 or A1R; Nikon) at RT. For experiments at high temperature (the restrictive temperature for shi^{ts1}), we preincubated dissected larvae in warm (33°C) HL-3 for 2 min after incubation with FlAsH and washing in Bal and subsequently kept them on a heating plate during the experiment to maintain 33°C. Photoinactivated synapses were analyzed on muscles 12 and 13.

To visualize FlAsH, preparations were treated as in the previous paragraph but without the photoinactivation step. Imaging of FlAsH fluorescence was performed on a confocal microscope (LSM 510 Meta; Carl Zeiss) using a 63×, 1.0 NA water immersion lens (zoom 4) at RT.

Electrophysiology

Two electrode voltage clamp experiments (holding potential at −70 mV) to record EJCs were performed in HL-3 with $CaCl_2$ as indicated (Verstreken et al., 2009; Khuong et al., 2010), and miniatures were recorded in the presence of 0.5 mM $CaCl_2$ and 0.5 µM tetrodotoxin (Sigma-Aldrich). The holding potential was −70 mV, and the input resistance of the muscles was ≥4 MΩ. Current clamp experiments to record EJPs were performed in HL-3 with 2 mM $CaCl_2$ from muscle 6, segment A2 or A3. Motor neurons were stimulated using a suction electrode at ∼2× threshold. EJC and EJP measurements were amplified with an amplifier (Axoclamp 900A; Axon instruments), digitized with a Digidata 1440A (Axon instruments), and stored and processed using Clampex 10.2 (Axon instruments). Data were Bessel filtered at 1 kHz.

Fluorescence imaging and quantification

FM 1-43 labeling was performed by incubating dissected larvae either in HL-3 with 4 µM FM 1-43 (Invitrogen), 1.5 mM $CaCl_2$, and 90 mM KCl for 5 min (1 min for EndoA) or in HL-3 with 1.5 mM $CaCl_2$ and electrically stimulating motor nerves at 10 Hz for 5 min. Subsequently, noninternalized dye was removed by washing with HL-3. For unloading, nerve terminals were stimulated for a second time in HL-3 with 90 mM KCl for 10 min and washed with HL-3 before imaging. For experiments at high temperature (restrictive temperature for shi^{ts1}), dissected fillets were kept on a heating plate during the experiment to maintain 33°C. Quantifications of the FM 1-43 intensity in unloading experiments were corrected for bleaching by multiplying the intensity value by the bleaching coefficient (calculated from imaging twice the same NMJ of *yw* controls). Images of FM 1-43 were captured with a confocal microscope (LSM 510 Meta) and 63×, 1.0 NA water immersion lens (zoom 4) or with a confocal microscope (A1R) and a 60×, 1.0 NA water immersion lens (zoom 4) at RT and stored using LSM 510 or NIS elements AR 4.13 software packages (Nikon), respectively. For quantification of intensities, the mean fluorescence levels in individual boutons minus the background fluorescence in muscles was calculated and averaged. To score accumulations of FM 1-43 inside boutons, samples were blinded, and such structures were manually counted and normalized to the bouton surface area (measured in Fiji; National Institutes of Health). Boutons on muscles 12 and 13 were imaged and analyzed.

For immunohistochemistry, larvae were dissected in HL-3 and fixed in 4% formaldehyde for 20 min. Samples were permeabilized in 0.4% Triton X-100 and incubated overnight at 4°C with the following antibodies: mouse anti–disc large (DLG) at 1:50 raised against the second PDZ domain of DLG (Parnas et al., 2001), rabbit anti-HRP at 1:2,000 (Jackson ImmunoResearch Laboratories, Inc.), mouse anti-HA at 1:500 (Eurogentec), mouse anti-Dynamin at 1:50 (BD), and rabbit anti–α-Ada (1:500) raised against the 360 C-terminal amino acid sequence of *Drosophila* α-Ada (González-Gaitán and Jäckle, 1997). After washes with PBS, Alexa Fluor 488– and 555–conjugated secondary antibodies (Invitrogen) were added at 1:500 for 2 h at RT, washed, and mounted in Vectashield (Vector Laboratories). Images were captured either on a confocal microscope (LSM 510 META) with a 63×, NA 1.4 oil lens or on a confocal microscope (A1R) with a 60×, 1.4 NA oil lens (zoom 1 and 4) and stored using LSM 510 or NIS elements AR 4.13 software packages, respectively. All images were taken

at RT. Labeling intensity in single section confocal images was quantified as the mean gray value of boutonic fluorescence corrected for background in the muscle. Furthermore, NMJ length and bouton number were quantified by manually tracing the NMJ branches in Fiji and summing them to calculate the total length and by manually counting the individual boutons, respectively. The bouton surface area was measured by tracing the circumference of images taken from the muscle (Coyle et al., 2004).

Superresolution structural illumination microscopy images were acquired on a microscope (Elyra S.1; Carl Zeiss) using a 63×, NA 1.4 oil lens and three rotations at RT, and images were processed and stored using ZEN 2011 software (Carl Zeiss). To quantify the mean distribution of HA-Chc or α-Ada labeling intensity over several boutons, we selected boutons of similar size but still first needed to rescale the size of each bouton to a standard diameter as to be able to average the HA-Chc or α-Ada labeling intensities per position along the bouton diameters. We therefore resized all the boutons that entered quantification to a width of 500 pixels using the bicubic interpolation tool in Photoshop (Adobe). We then defined the line intensities at the center of each bouton (to avoid artifacts, the mean intensity of the 45 pixels above and below the line) along these 500 pixels as to obtain a line scan view of the intensity profile through the center of a bouton (line width and plot profile tools in Fiji). Finally, to obtain the mean labeling distribution across boutons, we calculated the mean intensity for each point along the 500 pixels.

EM

TEM was performed on dissected larvae in HL-3 with 1.5 mM $CaCl_2$ stimulated with 60 mM KCl for 5 min. Preparations were briefly washed and then fixed for 2 h at RT and then overnight at 4°C in 4% paraformaldehyde and 1% glutaraldehyde in 0.1 M Na-cacodylate buffer with 1 mM $MgCl_2$ at pH 7.2. For samples in which proteins were inactivated by FlAsH-FALI, the relevant segments were trimmed. Samples were washed in 0.1 M Na-cacodylate buffer, osmicated in fresh 1% OsO_4 in 0.1 M Na-cacodylate for 2 h on ice, and then washed in cold water. Next, the tissue was stained with aqueous 2% uranyl acetate for 1.5 h, dehydrated in a series of ethanol, and embedded in Agar 100. Ultrathin 70-nm sections were cut with an ultramicrotome (EM UC7; Leica) and visualized at the EM core facility KU Leuven using a transmission electron microscope (JEM-1400; JEOL) operated at 80 kV. Micrographs were acquired using a bottom-mounted camera (Quemesa; 11 megapixels; Olympus) and a side-mounted camera (Veleta; 4 megapixels; Olympus) using iTEM 5.2 software (Olympus). The used magnifications were 10,000 and 20,000× with the Quemesa and 30,000 and 50,000× with the Veleta camera. Quantification of ultrastructural features was performed using Fiji and iTEM 5.2. For experiments that were executed at high temperature photoinactivation, stimulation and washing steps were performed at 33°C (see the section Photoinactivation of Shi-4C and Endo-4C and visualization of FlAsH fluorescence of the Materials and methods). Subsequently, the primary fixation was first performed for 20 min at 33°C.

For electron tomography tilt series, micrographs at 200 kV and 10,000× were obtained from 200–300-nm-thick sections collected on Formvar carbon-coated grids covered with colloidal gold particles (15 nm) using an electron microscope (JEM-2100; JEOL). Micrographs were recorded from −60 to 60° at 2° intervals using Recorder software (JEOL) and a 1,024 × 1,024–pixel bottom-mounted charge-coupled device camera (MultiScan; Gatan). Tomograms were generated with the eTomo module in IMOD, using the gold particles for alignment. 3D models were built by semiautomated surface rendering and computed using 3dmod in IMOD.

Image processing

Individual color channels were merged using Fiji, and images were adjusted for brightness and contrast using Photoshop 7.

Statistical analysis

Statistical analysis was performed using the appropriate statistical test (*t* test or analysis of variance [ANOVA] with Tukey's test) for comparisons between groups, as described in the figure legends. The statistical significance of differences was defined with a $P < 0.05$.

Online supplemental material

Fig. S1 shows that *dynamin*-null mutants that express the tetracysteine-tagged Dynamin do not show overt behavioral defects and normal third instar larval morphology. Fig. S2 shows TEM micrographs of boutons from animals that express RNAi to down-regulate Dynamin expression in the nervous system. Fig. S3 shows a series of superresolution z stacks of Chc and α-Ada labeling in boutons in which Dynamin was or was not inactivated and that were stimulated or not stimulated using KCl (see also Fig. 5). Fig. S4 shows a series of superresolution z stacks of Chc and α-Ada labeling in boutons in which Dynamin was or was not down-regulated by RNAi and that were stimulated or not stimulated using KCl. Fig. S5 shows that when Shi-4C is expressed in a wild-type background, photoinactivation results in a loss of Dynamin function despite the presence of wild-type Dynamin. Table S1 contains all the primers used to generate the Shi-4C, Endo-4C, and HA-Chc constructs. Video 1 shows digital sections through the tomographic reconstruction shown in Fig. 7. Online supplemental material is available at http://www.jcb.org/cgi/content/full/jcb.201310090/DC1.

We thank the Bloomington Drosophila Stock Center, the Vienna Drosophila RNAi center, the Drosophila Genomics Resource Center, and the Developmental Studies Hybridoma Bank; B. André, H. Bellen, M. Cousin, M. González-Gaitán, B. Hassan, E. Lauwers, V. Morais, M. Ramaswami, J. Slabbaert, and D. Schmucker; and members of the Verstreken laboratory for reagents, help, or comments. We thank S. Munck and N. Corthout from the VIB Bio Imaging Core, Light Microscopy and Imaging Network facility, and KU Leuven Cell Imaging Core and P. Baatsen from the KU Leuven EM core facility and VIB Center for the Biology of Disease.

Support to P. Verstreken was provided by a European Research Council Starting Grant (260678), the Research Foundation Flanders (grants G053913, G079013, G095511, and G074709), the Hercules Foundation, the Instituut voor Wetenschap en Technologie, the Interuniversity Attraction Pole program by the Belgian Federal Science Policy Office, the research fund KU Leuven, and VIB.

The authors declare no competing financial interests.

Submitted: 21 October 2013
Accepted: 26 February 2014

References

Aguet, F., C.N. Antonescu, M. Mettlen, S.L. Schmid, and G. Danuser. 2013. Advances in analysis of low signal-to-noise images link dynamin and AP2 to the functions of an endocytic checkpoint. *Dev. Cell*. 26:279–291. http://dx.doi.org/10.1016/j.devcel.2013.06.019

Anggono, V., K.J. Smillie, M.E. Graham, V.A. Valova, M.A. Cousin, and P.J. Robinson. 2006. Syndapin I is the phosphorylation-regulated dynamin I partner in synaptic vesicle endocytosis. *Nat. Neurosci.* 9:752–760. http://dx.doi.org/10.1038/nn1695

Bashkirov, P.V., S.A. Akimov, A.I. Evseev, S.L. Schmid, J. Zimmerberg, and V.A. Frolov. 2008. GTPase cycle of dynamin is coupled to membrane squeeze and release, leading to spontaneous fission. *Cell*. 135:1276–1286. http://dx.doi.org/10.1016/j.cell.2008.11.028

Bazinet, C., A.L. Katzen, M. Morgan, A.P. Mahowald, and S.K. Lemmon. 1993. The *Drosophila* clathrin heavy chain gene: clathrin function is essential in a multicellular organism. *Genetics*. 134:1119–1134.

Bethoney, K.A., M.C. King, J.E. Hinshaw, E.M. Ostap, and M.A. Lemmon. 2009. A possible effector role for the pleckstrin homology (PH) domain of dynamin. *Proc. Natl. Acad. Sci. USA*. 106:13359–13364. http://dx.doi.org/10.1073/pnas.0906945106

Betz, W.J., F. Mao, and C.B. Smith. 1996. Imaging exocytosis and endocytosis. *Curr. Opin. Neurobiol.* 6:365–371. http://dx.doi.org/10.1016/S0959-4388(96)80121-8

Cao, H., F. Garcia, and M.A. McNiven. 1998. Differential distribution of dynamin isoforms in mammalian cells. *Mol. Biol. Cell*. 9:2595–2609. http://dx.doi.org/10.1091/mbc.9.9.2595

Chappie, J.S., S. Acharya, M. Leonard, S.L. Schmid, and F. Dyda. 2010. G domain dimerization controls dynamin's assembly-stimulated GTPase activity. *Nature*. 465:435–440. http://dx.doi.org/10.1038/nature09032

Chen, M.L., D. Green, L. Liu, Y.C. Lam, L. Mukai, S. Rao, S. Ramagiri, K.S. Krishnan, J.E. Engel, J.J. Lin, and C.F. Wu. 2002. Unique biochemical and behavioral alterations in *Drosophila* shibire(ts1) mutants imply a conformational state affecting dynamin subcellular distribution and synaptic vesicle cycling. *J. Neurobiol.* 53:319–329. http://dx.doi.org/10.1002/neu.10101

Chen, M.S., R.A. Obar, C.C. Schroeder, T.W. Austin, C.A. Poodry, S.C. Wadsworth, and R.B. Vallee. 1991. Multiple forms of dynamin are encoded by shibire, a *Drosophila* gene involved in endocytosis. *Nature*. 351:583–586. http://dx.doi.org/10.1038/351583a0

Clayton, E.L., V. Anggono, K.J. Smillie, N. Chau, P.J. Robinson, and M.A. Cousin. 2009. The phospho-dependent dynamin-syndapin interaction triggers activity-dependent bulk endocytosis of synaptic vesicles. *J. Neurosci.* 29:7706–7717. http://dx.doi.org/10.1523/JNEUROSCI.1976-09.2009

Clayton, E.L., N. Sue, K.J. Smillie, T. O'Leary, N. Bache, G. Cheung, A.R. Cole, D.J. Wyllie, C. Sutherland, P.J. Robinson, and M.A. Cousin. 2010. Dynamin I phosphorylation by GSK3 controls activity-dependent bulk endocytosis of synaptic vesicles. *Nat. Neurosci.* 13:845–851. http://dx.doi.org/10.1038/nn.2571

Conner, S.D., and S.L. Schmid. 2003. Regulated portals of entry into the cell. *Nature*. 422:37–44. http://dx.doi.org/10.1038/nature01451

Coyle, I.P., Y.H. Koh, W.C. Lee, J. Slind, T. Fergestad, J.T. Littleton, and B. Ganetzky. 2004. Nervous wreck, an SH3 adaptor protein that interacts with Wsp, regulates synaptic growth in *Drosophila*. *Neuron*. 41:521–534. http://dx.doi.org/10.1016/S0896-6273(04)00016-9

Damke, H., D.D. Binns, H. Ueda, S.L. Schmid, and T. Baba. 2001. Dynamin GTPase domain mutants block endocytic vesicle formation at morphologically distinct stages. *Mol. Biol. Cell*. 12:2578–2589. http://dx.doi.org/10.1091/mbc.12.9.2578

David, C., P.S. McPherson, O. Mundigl, and P. de Camilli. 1996. A role of amphiphysin in synaptic vesicle endocytosis suggested by its binding to dynamin in nerve terminals. *Proc. Natl. Acad. Sci. USA*. 93:331–335. http://dx.doi.org/10.1073/pnas.93.1.331

Delgado, R., C. Maureira, C. Oliva, Y. Kidokoro, and P. Labarca. 2000. Size of vesicle pools, rates of mobilization, and recycling at neuromuscular synapses of a *Drosophila* mutant, shibire. *Neuron*. 28:941–953. http://dx.doi.org/10.1016/S0896-6273(00)00165-3

Estes, P.S., J. Roos, A. van der Bliek, R.B. Kelly, K.S. Krishnan, and M. Ramaswami. 1996. Traffic of dynamin within individual *Drosophila* synaptic boutons relative to compartment-specific markers. *J. Neurosci.* 16:5443–5456.

Evans, G.J., and M.A. Cousin. 2007. Activity-dependent control of slow synaptic vesicle endocytosis by cyclin-dependent kinase 5. *J. Neurosci.* 27:401–411. http://dx.doi.org/10.1523/JNEUROSCI.3809-06.2007

Ferguson, S.M., and P. De Camilli. 2012. Dynamin, a membrane-remodelling GTPase. *Nat. Rev. Mol. Cell Biol.* 13:75–88.

Ferguson, S.M., G. Brasnjo, M. Hayashi, M. Wölfel, C. Collesi, S. Giovedi, A. Raimondi, L.W. Gong, P. Ariel, S. Paradise, et al. 2007. A selective activity-dependent requirement for dynamin 1 in synaptic vesicle endocytosis. *Science*. 316:570–574. http://dx.doi.org/10.1126/science.1140621

Ferguson, S.M., A. Raimondi, S. Paradise, H. Shen, K. Mesaki, A. Ferguson, O. Destaing, G. Ko, J. Takasaki, O. Cremona, et al. 2009. Coordinated actions of actin and BAR proteins upstream of dynamin at endocytic clathrin-coated pits. *Dev. Cell*. 17:811–822. http://dx.doi.org/10.1016/j.devcel.2009.11.005

Ford, M.G., S. Jenni, and J. Nunnari. 2011. The crystal structure of dynamin. *Nature*. 477:561–566. http://dx.doi.org/10.1038/nature10441

Gao, S., A. von der Malsburg, S. Paeschke, J. Behlke, O. Haller, G. Kochs, and O. Daumke. 2010. Structural basis of oligomerization in the stalk region of dynamin-like MxA. *Nature*. 465:502–506. http://dx.doi.org/10.1038/nature08972

González-Gaitán, M., and H. Jäckle. 1997. Role of *Drosophila* α-adaptin in presynaptic vesicle recycling. *Cell*. 88:767–776. http://dx.doi.org/10.1016/S0092-8674(00)81923-6

Grant, D., S. Unadkat, A. Katzen, K.S. Krishnan, and M. Ramaswami. 1998. Probable mechanisms underlying interallelic complementation and temperature-sensitivity of mutations at the shibire locus of *Drosophila melanogaster*. *Genetics*. 149:1019–1030.

Gu, M., Q. Liu, S. Watanabe, L. Sun, G. Hollopeter, B.D. Grant, and E.M. Jorgensen. 2013. AP2 hemicomplexes contribute independently to synaptic vesicle endocytosis. *Elife*. 2:e00190. http://dx.doi.org/10.7554/eLife.00190

Hayashi, M., A. Raimondi, E. O'Toole, S. Paradise, C. Collesi, O. Cremona, S.M. Ferguson, and P. De Camilli. 2008. Cell- and stimulus-dependent heterogeneity of synaptic vesicle endocytic recycling mechanisms revealed by studies of dynamin 1-null neurons. *Proc. Natl. Acad. Sci. USA*. 105:2175–2180. http://dx.doi.org/10.1073/pnas.0712171105

Heerssen, H., R.D. Fetter, and G.W. Davis. 2008. Clathrin dependence of synaptic-vesicle formation at the *Drosophila* neuromuscular junction. *Curr. Biol.* 18:401–409. http://dx.doi.org/10.1016/j.cub.2008.02.055

Holt, M., A. Cooke, M.M. Wu, and L. Lagnado. 2003. Bulk membrane retrieval in the synaptic terminal of retinal bipolar cells. *J. Neurosci.* 23:1329–1339.

Kasprowicz, J., S. Kuenen, K. Miskiewicz, R.L. Habets, L. Smitz, and P. Verstreken. 2008. Inactivation of clathrin heavy chain inhibits synaptic recycling but allows bulk membrane uptake. *J. Cell Biol.* 182:1007–1016. http://dx.doi.org/10.1083/jcb.200804162

Khuong, T.M., R.L. Habets, J.R. Slabbaert, and P. Verstreken. 2010. WASP is activated by phosphatidylinositol-4,5-bisphosphate to restrict synapse growth in a pathway parallel to bone morphogenetic protein signaling. *Proc. Natl. Acad. Sci. USA*. 107:17379–17384. http://dx.doi.org/10.1073/pnas.1001794107

Khuong, T.M., R.L. Habets, S. Kuenen, A. Witkowska, J. Kasprowicz, J. Swerts, R. Jahn, G. van den Bogaart, and P. Verstreken. 2013. Synaptic PI(3,4,5)P3 is required for Syntaxin1A clustering and neurotransmitter release. *Neuron*. 77:1097–1108. http://dx.doi.org/10.1016/j.neuron.2013.01.025

Kitamoto, T. 2001. Conditional modification of behavior in *Drosophila* by targeted expression of a temperature-sensitive shibire allele in defined neurons. *J. Neurobiol.* 47:81–92. http://dx.doi.org/10.1002/neu.1018

Koenig, J.H., and K. Ikeda. 1989. Disappearance and reformation of synaptic vesicle membrane upon transmitter release observed under reversible blockage of membrane retrieval. *J. Neurosci.* 9:3844–3860.

Koh, T.W., P. Verstreken, and H.J. Bellen. 2004. Dap160/intersectin acts as a stabilizing scaffold required for synaptic development and vesicle endocytosis. *Neuron*. 43:193–205. http://dx.doi.org/10.1016/j.neuron.2004.06.029

Liu, S.H., M.S. Marks, and F.M. Brodsky. 1998. A dominant-negative clathrin mutant differentially affects trafficking of molecules with distinct sorting motifs in the class II major histocompatibility complex (MHC) pathway. *J. Cell Biol.* 140:1023–1037. http://dx.doi.org/10.1083/jcb.140.5.1023

Liu, Y.W., S. Neumann, R. Ramachandran, S.M. Ferguson, T.J. Pucadyil, and S.L. Schmid. 2011. Differential curvature sensing and generating activities of dynamin isoforms provide opportunities for tissue-specific regulation. *Proc. Natl. Acad. Sci. USA*. 108:E234–E242. http://dx.doi.org/10.1073/pnas.1102710108

Loerke, D., M. Mettlen, D. Yarar, K. Jaqaman, H. Jaqaman, G. Danuser, and S.L. Schmid. 2009. Cargo and dynamin regulate clathrin-coated pit maturation. *PLoS Biol.* 7:e57. http://dx.doi.org/10.1371/journal.pbio.1000057

LoGiudice, L., and G. Matthews. 2006. The synaptic vesicle cycle: is kissing overrated? *Neuron*. 51:676–677. http://dx.doi.org/10.1016/j.neuron.2006.09.004

Macia, E., M. Ehrlich, R. Massol, E. Boucrot, C. Brunner, and T. Kirchhausen. 2006. Dynasore, a cell-permeable inhibitor of dynamin. *Dev. Cell*. 10:839–850. http://dx.doi.org/10.1016/j.devcel.2006.04.002

Marek, K.W., and G.W. Davis. 2002. Transgenically encoded protein photoinactivation (FlAsH-FALI): acute inactivation of synaptotagmin I. *Neuron*. 36:805–813. http://dx.doi.org/10.1016/S0896-6273(02)01068-1

Marie, B., S.T. Sweeney, K.E. Poskanzer, J. Roos, R.B. Kelly, and G.W. Davis. 2004. Dap160/intersectin scaffolds the periactive zone to achieve high-fidelity endocytosis and normal synaptic growth. *Neuron*. 43:207–219. http://dx.doi.org/10.1016/j.neuron.2004.07.001

Marks, B., M.H. Stowell, Y. Vallis, I.G. Mills, A. Gibson, C.R. Hopkins, and H.T. McMahon. 2001. GTPase activity of dynamin and resulting conformation change are essential for endocytosis. *Nature*. 410:231–235. http://dx.doi.org/10.1038/35065645

Martin, B.R., B.N. Giepmans, S.R. Adams, and R.Y. Tsien. 2005. Mammalian cell-based optimization of the biarsenical-binding tetracysteine motif for improved fluorescence and affinity. *Nat. Biotechnol.* 23:1308–1314. http://dx.doi.org/10.1038/nbt1136

McMahon, H.T., and E. Boucrot. 2011. Molecular mechanism and physiological functions of clathrin-mediated endocytosis. *Nat. Rev. Mol. Cell Biol.* 12:517–533. http://dx.doi.org/10.1038/nrm3151

McNiven, M.A., H. Cao, K.R. Pitts, and Y. Yoon. 2000. The dynamin family of mechanoenzymes: pinching in new places. *Trends Biochem. Sci.* 25:115–120. http://dx.doi.org/10.1016/S0968-0004(99)01538-8

Merhi, A., N. Gérard, E. Lauwers, M. Prévost, and B. André. 2011. Systematic mutational analysis of the intracellular regions of yeast Gap1 permease. *PLoS ONE*. 6:e18457. http://dx.doi.org/10.1371/journal.pone.0018457

Merrifield, C.J., M.E. Feldman, L. Wan, and W. Almers. 2002. Imaging actin and dynamin recruitment during invagination of single clathrin-coated pits. *Nat. Cell Biol.* 4:691–698. http://dx.doi.org/10.1038/ncb837

Mettlen, M., M. Stoeber, D. Loerke, C.N. Antonescu, G. Danuser, and S.L. Schmid. 2009. Endocytic accessory proteins are functionally distinguished by their differential effects on the maturation of clathrin-coated pits. *Mol. Biol. Cell*. 20:3251–3260. http://dx.doi.org/10.1091/mbc.E09-03-0256

Narayanan, R., M. Leonard, B.D. Song, S.L. Schmid, and M. Ramaswami. 2005. An internal GAP domain negatively regulates presynaptic dynamin in vivo: a two-step model for dynamin function. *J. Cell Biol.* 169:117–126. http://dx.doi.org/10.1083/jcb.200502042

Newton, A.J., T. Kirchhausen, and V.N. Murthy. 2006. Inhibition of dynamin completely blocks compensatory synaptic vesicle endocytosis. *Proc. Natl. Acad. Sci. USA*. 103:17955–17960. http://dx.doi.org/10.1073/pnas.0606212103

Nonet, M.L., A.M. Holgado, F. Brewer, C.J. Serpe, B.A. Norbeck, J. Holleran, L. Wei, E. Hartwieg, E.M. Jorgensen, and A. Alfonso. 1999. UNC-11, a *Caenorhabditis elegans* AP180 homologue, regulates the size and protein composition of synaptic vesicles. *Mol. Biol. Cell*. 10:2343–2360. http://dx.doi.org/10.1091/mbc.10.7.2343

Okamoto, P.M., J.S. Herskovits, and R.B. Vallee. 1997. Role of the basic, proline-rich region of dynamin in Src homology 3 domain binding and endocytosis. *J. Biol. Chem.* 272:11629–11635. http://dx.doi.org/10.1074/jbc.272.17.11629

Park, R.J., H. Shen, L. Liu, X. Liu, S.M. Ferguson, and P. De Camilli. 2013. Dynamin triple knockout cells reveal off target effects of commonly used dynamin inhibitors. *J. Cell Sci.* 126:5305–5312. http://dx.doi.org/10.1242/jcs.138578

Parnas, D., A.P. Haghighi, R.D. Fetter, S.W. Kim, and C.S. Goodman. 2001. Regulation of postsynaptic structure and protein localization by the Rho-type guanine nucleotide exchange factor dPix. *Neuron*. 32:415–424. http://dx.doi.org/10.1016/S0896-6273(01)00485-8

Poskanzer, K.E., K.W. Marek, S.T. Sweeney, and G.W. Davis. 2003. Synaptotagmin I is necessary for compensatory synaptic vesicle endocytosis in vivo. *Nature*. 426:559–563. http://dx.doi.org/10.1038/nature02184

Puthenveedu, M.A., and M. von Zastrow. 2006. Cargo regulates clathrin-coated pit dynamics. *Cell*. 127:113–124. http://dx.doi.org/10.1016/j.cell.2006.08.035

Qualmann, B., J. Roos, P.J. DiGregorio, and R.B. Kelly. 1999. Syndapin I, a synaptic dynamin-binding protein that associates with the neural Wiskott-Aldrich syndrome protein. *Mol. Biol. Cell*. 10:501–513. http://dx.doi.org/10.1091/mbc.10.2.501

Raimondi, A., S.M. Ferguson, X. Lou, M. Armbruster, S. Paradise, S. Giovedi, M. Messa, N. Kono, J. Takasaki, V. Cappello, et al. 2011. Overlapping role of dynamin isoforms in synaptic vesicle endocytosis. *Neuron*. 70:1100–1114. http://dx.doi.org/10.1016/j.neuron.2011.04.031

Ramaswami, M., K.S. Krishnan, and R.B. Kelly. 1994. Intermediates in synaptic vesicle recycling revealed by optical imaging of *Drosophila* neuromuscular junctions. *Neuron*. 13:363–375. http://dx.doi.org/10.1016/0896-6273(94)90353-0

Roux, A., K. Uyhazi, A. Frost, and P. De Camilli. 2006. GTP-dependent twisting of dynamin implicates constriction and tension in membrane fission. *Nature*. 441:528–531. http://dx.doi.org/10.1038/nature04718

Simpson, F., N.K. Hussain, B. Qualmann, R.B. Kelly, B.K. Kay, P.S. McPherson, and S.L. Schmid. 1999. SH3-domain-containing proteins function at distinct steps in clathrin-coated vesicle formation. *Nat. Cell Biol.* 1:119–124.

Smillie, K.J., and M.A. Cousin. 2012. Akt/PKB controls the activity-dependent bulk endocytosis of synaptic vesicles. *Traffic*. 13:1004–1011. http://dx.doi.org/10.1111/j.1600-0854.2012.01365.x

Stewart, B.A., H.L. Atwood, J.J. Renger, J. Wang, and C.F. Wu. 1994. Improved stability of *Drosophila* larval neuromuscular preparations in haemolymph-like physiological solutions. *J. Comp. Physiol. A Neuroethol. Sens. Neural Behav. Physiol.* 175:179–191. http://dx.doi.org/10.1007/BF00215114

Sundborger, A., C. Soderblom, O. Vorontsova, E. Evergren, J.E. Hinshaw, and O. Shupliakov. 2011. An endophilin-dynamin complex promotes budding of clathrin-coated vesicles during synaptic vesicle recycling. *J. Cell Sci.* 124:133–143. http://dx.doi.org/10.1242/jcs.072686

van der Bliek, A.M., and E.M. Meyerowitz. 1991. Dynamin-like protein encoded by the *Drosophila* shibire gene associated with vesicular traffic. *Nature*. 351:411–414. http://dx.doi.org/10.1038/351411a0

Venken, K.J., Y. He, R.A. Hoskins, and H.J. Bellen. 2006. P[acman]: a BAC transgenic platform for targeted insertion of large DNA fragments in *D. melanogaster*. *Science*. 314:1747–1751. http://dx.doi.org/10.1126/science.1134426

Venken, K.J., J. Kasprowicz, S. Kuenen, J. Yan, B.A. Hassan, and P. Verstreken. 2008. Recombineering-mediated tagging of *Drosophila* genomic constructs for in vivo localization and acute protein inactivation. *Nucleic Acids Res.* 36:e114. http://dx.doi.org/10.1093/nar/gkn486

Verstreken, P., O. Kjaerulff, T.E. Lloyd, R. Atkinson, Y. Zhou, I.A. Meinertzhagen, and H.J. Bellen. 2002. Endophilin mutations block clathrin-mediated endocytosis but not neurotransmitter release. *Cell*. 109:101–112. http://dx.doi.org/10.1016/S0092-8674(02)00688-8

Verstreken, P., C.V. Ly, K.J. Venken, T.W. Koh, Y. Zhou, and H.J. Bellen. 2005. Synaptic mitochondria are critical for mobilization of reserve pool vesicles at *Drosophila* neuromuscular junctions. *Neuron*. 47:365–378. http://dx.doi.org/10.1016/j.neuron.2005.06.018

Verstreken, P., T. Ohyama, C. Haueter, R.L. Habets, Y.Q. Lin, L.E. Swan, C.V. Ly, K.J. Venken, P. De Camilli, and H.J. Bellen. 2009. Tweek, an evolutionarily conserved protein, is required for synaptic vesicle recycling. *Neuron*. 63:203–215. http://dx.doi.org/10.1016/j.neuron.2009.06.017

Watanabe, S., B.R. Rost, M. Camacho-Pérez, M.W. Davis, B. Söhl-Kielczynski, C. Rosenmund, and E.M. Jorgensen. 2013. Ultrafast endocytosis at mouse hippocampal synapses. *Nature*. 504:242–247. http://dx.doi.org/10.1038/nature12809

Winther, A.M., W. Jiao, O. Vorontsova, K.A. Rees, T.W. Koh, E. Sopova, K.L. Schulze, H.J. Bellen, and O. Shupliakov. 2013. The dynamin-binding domains of Dap160/intersectin affect bulk membrane retrieval in synapses. *J. Cell Sci.* 126:1021–1031. http://dx.doi.org/10.1242/jcs.118968

Wu, X.S., B.D. McNeil, J. Xu, J. Fan, L. Xue, E. Melicoff, R. Adachi, L. Bai, and L.G. Wu. 2009. Ca(2+) and calmodulin initiate all forms of endocytosis during depolarization at a nerve terminal. *Nat. Neurosci.* 12:1003–1010. http://dx.doi.org/10.1038/nn.2355

Yan, P., Y. Xiong, B. Chen, S. Negash, T.C. Squier, and M.U. Mayer. 2006. Fluorophore-assisted light inactivation of calmodulin involves singlet-oxygen mediated cross-linking and methionine oxidation. *Biochemistry*. 45:4736–4748. http://dx.doi.org/10.1021/bi052395a

Zhang, B., Y.H. Koh, R.B. Beckstead, V. Budnik, B. Ganetzky, and H.J. Bellen. 1998. Synaptic vesicle size and number are regulated by a clathrin adaptor protein required for endocytosis. *Neuron*. 21:1465–1475. http://dx.doi.org/10.1016/S0896-6273(00)80664-9